Tellus (1995), 47A, 1–29
Printed in Belgium – all rights reserved

TELLUS
ISSN 0280–6495

Incipient explosive marine cyclogenesis: coastal development

By LANCE F. BOSART[1]*, CHUNG-CHIENG LAI[2] and ERIC ROGERS[3], [1]*Department of Atmospheric Science, State University of New York at Albany, 1400 Washington Avenue, Albany, New York 12222, USA*; [2]*Geoanalysis Group, EES-5, MS-D401, Earth and Environmental Science Division, Los Alamos National Laboratory, Los Alamos, NM 87545, USA*; [3]*National Meteorological Center, W/NMC-22-WWB-Room 204, Washington, DC 20233, USA*

(Manuscript received 3 September 1993; in final form 31 January 1994)

ABSTRACT

A case of incipient explosive marine cyclogenesis along the east coast of North America from February 1974 is investigated. The cyclone was noteworthy for deepening 36 mb in 15 h as it crossed a region of anomalously warm sea surface temperatures beneath a very favorable flow configuration aloft for explosive development. The precyclogenetic environment featured coastal frontogenesis and cyclonic vorticity production in association with oceanic sensible and latent heat fluxes in the westward-flowing air in advance of the cyclone. The resulting relatively high values of surface vorticity in the coastal baroclinic zone probably helped to contribute to the intensity of the ensuing cyclogenesis, as a peak cyclonic vorticity tendency of $\sim 30 \times 10^{-9}\ \mathrm{s}^{-2}$ was computed in the coastal baroclinic zone at the time of most rapid surface intensification.

1. Introduction

Explosively deepening cyclones have been thoroughly studied since the seminal Sanders and Gyakum (1980) paper documented the preference for such storms to develop over the western ocean basins of the Northern Hemisphere. Subsequently, numerous authors have looked at various observational, theoretical and numerical aspects of the explosive cyclogenesis problem and the interested reader is urged to consult the excellent review papers from the Palmén Symposium by Reed (1990), Hoskins (1990), Uccellini (1990), Browning (1990), Shapiro and Keyser (1990), and Bengtsson (1990) for more information. The purpose of this paper is to document a case of explosive cyclogenesis along the east coast of North America (16–17 February 1974) that resulted from the interaction of transient disturbances embedded in separate jet streams aloft into a configuration favorable for sustaining deep ascent above a prominent coastal baroclinic zone. Given the extensive discussion of explosive cyclogenesis in the literature over the last decade, our research goals are very modest. Our approach is designed to complement the much more detailed numerical and diagnostic analyses of the life cycles of modern storms (see, e.g., Reed et al. 1993a, b, Nieman and Shapiro 1993, and Nieman et al. 1993) by focusing on the initial development stages of the 16–17 February 1974 storm. Finally, we will try to place the cyclone development into perspective within the spectrum of explosive cyclogenesis cases reported elsewhere in the literature and from which new research opportunities might possibly arise.

A map illustrating the storm track, central pressure and the composite sea surface temperature (SST) field is given in Fig. 1 for the 16–17 February 1974 storm. Noteworthy aspects of the cyclone development include: (1) a central pressure decrease from 1002 mb at 1800 UTC 16 February to an estimated 966 mb at 0900 UTC

* Corresponding author.

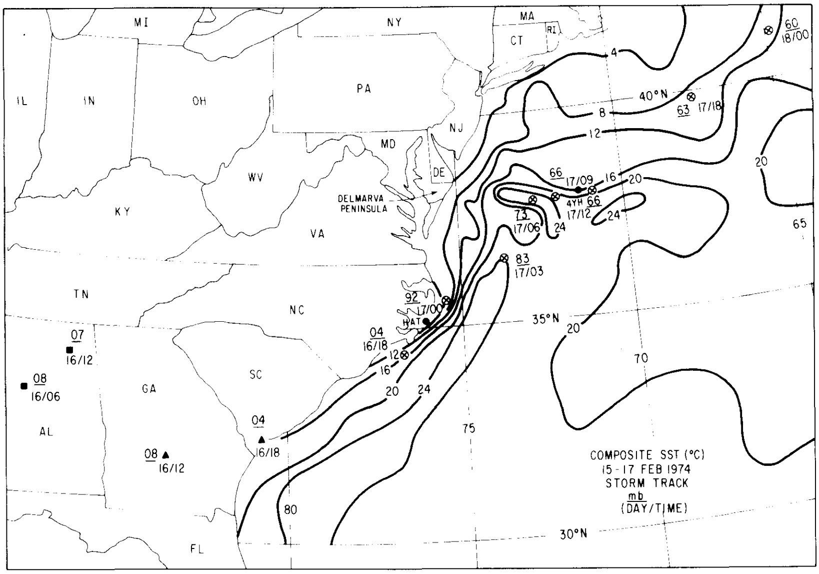

Fig. 1. Composite sea surface temperature (every 4°C) for the period 15–17 February 1974 and 6 h storm track position for the period 0600 UTC 16 February–0000 UTC 18 February 1974. Solid squares denote the location of the primary cyclone while the solid triangles and circles with a cross denote the secondary cyclone position. Day/time (UTC) and cyclone central pressure (underlined number in mb with leading 9 or 10 omitted) as shown. State 2-letter identifiers as shown.

17 February, a decrease of 36 mb in 15 h, and (2) the presence of +3 to +6°C SST anomalies and a warm ocean ring in the 35–40° N, 70–75° W latitude-longitude box through which the cyclone tracked. The positive SST anomalies in this region resulted from a Gulf Stream position farther north and west than usual (Gulf Stream, 1974a, b). Our detailed surface analyses will be restricted to the incipient cyclone development stage from 1800 UTC 16 February to 0000 UTC 17 February during which time coastal marine observations were relatively abundant. We will attempt to show that cyclogenesis occurred in a large scale environment that was reorganizing so as to favor the superposition of deep tropospheric ascent above a region of enhanced coastal baroclinicity and anomalously warm SST's.

2. Data and methodology

The surface and upper air analyses described in this paper were manually prepared and gridded. Surface land and marine (including ship log data) and upper air observations were extracted from the extensive research data base at the National Climatic Data Center (NCDC) of the United States and the National Center for Atmospheric Research (NCAR). These observations were hand plotted on surface and mandatory upper-level charts from which the manual analyses were prepared. Subsequently, these analyses were manually gridded with geopotential heights, temperatures, dew point temperatures, and wind direction and speed extracted on a one degree latitude-longitude mesh in support of the diagnostic calculations to follow. Inspection of the available surface observations from NCDC disclosed that significant numbers of land and marine observations (especially the latter) were not available in the NCAR database or the National Meteorological Center (NMC) operational data archives. Accordingly, we decided to pursue a manual analysis approach consistent with the limited goals of this study. The senior author was concerned that any resulting objective analyses ran the risk of containing significant inconsistencies in the horizontal and vertical structure of the flow near the Atlantic Ocean because of deficiencies in the relatively primitive analysis and initialization procedure then in use at NMC and upon which any first guess would be based.

3. Results

3.1. Surface analyses

Surface analyses for 1200 and 1800 UTC 16 February and 0000 and 0600 UTC 17 February appear in Figs. 2a–d. Prominent features at 1200 UTC (Fig. 2a) include a developing coastal baroclinic zone along the Carolina coast known locally as a coastal front (see, e.g., Bosart et al., 1972; Bosart, 1981; Riordan, 1990), a ridge of higher mean sea level pressure extending southwestward between the Appalachian Mountains and the coast, indicative of cold air damming (see, e.g., Baker, 1970; Richwein, 1980; Bosart, 1981; Forbes et al., 1987; Stauffer and Warner, 1987; Bell and Bosart, 1988), and an area of weak cyclonic circulation over northeastern Alabama and western Georgia with a pressure trough extending northward along the western slopes of the Appalachians as is frequently observed with southeasterly geostrophic flow in the lower troposphere (see, e.g., O'Handley and Bosart, 1989).

By 1800 UTC (Fig. 2b) twin cyclone centers define an elongated sea level pressure minimum along the Atlantic coast that is roughly coincident with the warm boundary of the coastal baroclinic zone. West of the Appalachians a remnant surface trough is apparent along the eastern edge of the warm air mass. The northeasternmost cyclone center is rapidly becoming the dominant storm as judged by the observed pressure falls in excess of 8 mb 3 h^{-1} along the coast. Also of interest is the wind shift line separating easterly from northeasterly flow that appears to be developing in the coastal waters northeast of the cyclone center as far north as New Jersey. This wind shift feature is marked by an inverted trough (trough in easterly flow) that builds northward to the south of the anticyclone centered over New England. The inverted trough marks a narrow tongue of warmer air that builds northward offshore while colder air remains trapped in the cold air damming region onshore. In effect, the coastal front is building northward along the warm boundary of the SST gradient marking the edge of the continental shelf waters (Fig. 1), a process that has also been described in a recent case study of oceanic cyclogenesis by Roebber (1993).

Explosive intensification is underway by 0000 UTC 17 February (Fig. 2c) with the cyclone center located near the extreme eastern coast of North Carolina at Cape Hatteras (HAT, 72304; see Fig. 1 for station locations). A 6 h deepening of 10–12 mb is estimated on the basis of the available data. Note the prominent narrow southerly jet (speeds in excess of 25 m s^{-1}) defined by two ship observations just ahead of the cold front near the cyclone center. This southerly jet is transporting warm, moist air northward toward the cyclone center. The cyclone center sits along the warm boundary of a coastal baroclinic zone that is estimated to be 6–7°C (100 km)$^{-1}$. Baroclinicity north of the cyclone center is maintained along the aforementioned coastal inverted trough. Finally, by 0600 UTC (Fig. 2d) the cyclone is deepening rapidly as it begins to move away from the coast. The estimated central pressure of 973 mb represents an additional 6 h deepening of $\sim$20 mb. Especially noteworthy are the large reported 3 h pressure falls from several ships and one buoy to the southwest of the cyclone center at this time. These pressure falls, located in the southwestern quadrant of a cyclone moving northeastward, are another indication of the extraordinary ongoing surface intensification.

3.2. Upper air analyses

The large scale flow pattern featured a broad trough over eastern North America and the western Atlantic Ocean, a ridge over western North America poleward of 30° N, and a low latitude trough south of the ridge at 1200 UTC 15 February 1974 (not shown). The associated split flow across western North America was marked by progressive individual short wave disturbances that entered the resulting confluent flow pattern downstream over central and eastern North America. At 300 mb jet streaks could be found from the vicinity of Hudson Bay to the eastern Great Lakes and from southern Texas eastward to almost the Atlantic coast between 30–35° N at 1200 UTC 15 February. Over the next 12 h, the northern jet strengthened and elongated in a confluent flow ahead of a migratory disturbance in the northern branch of the westerlies. The southern jet remained strong ahead of an advancing short wave disturbance in the southern branch

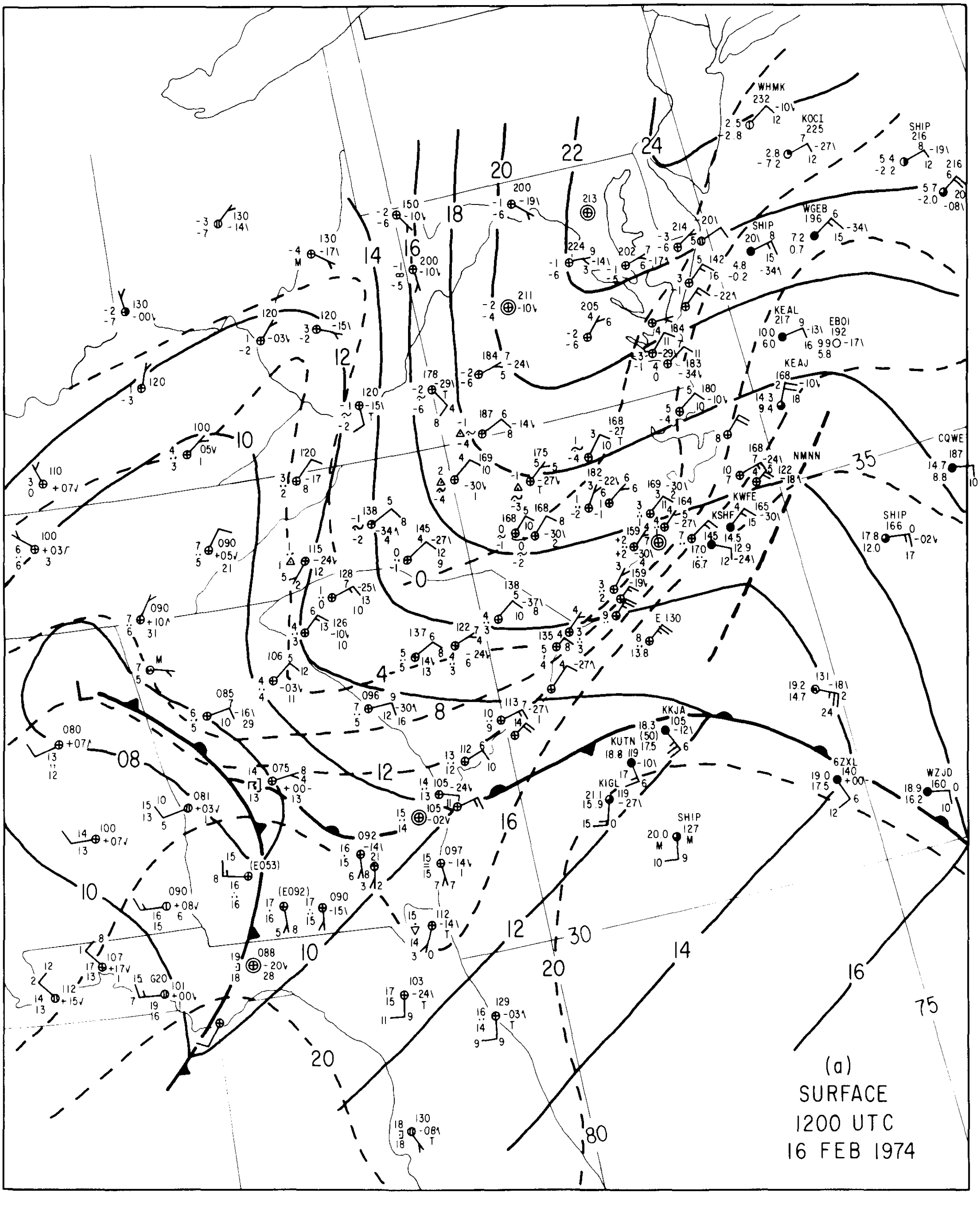

Fig. 2. Surface maps for (a) 1200 UTC 16 February 1974, (b) 1800 UTC 16 February 1974, (c) 0000 UTC 17 February 1974, and (d) 0600 UTC 17 February 1974. Isobars (solid) every 2 mb and isotherms (dashed) every 2°C (except every 4°C in panel a). Conventional plotting convention for surface data and frontal boundaries with bold dashed lines denoting coastal fronts. Winds in m s^{-1} with a pennant, full barb, and half barb denoting 25 m s^{-1}, 5 m s^{-1} and 2.5 m s^{-1}, respectively.

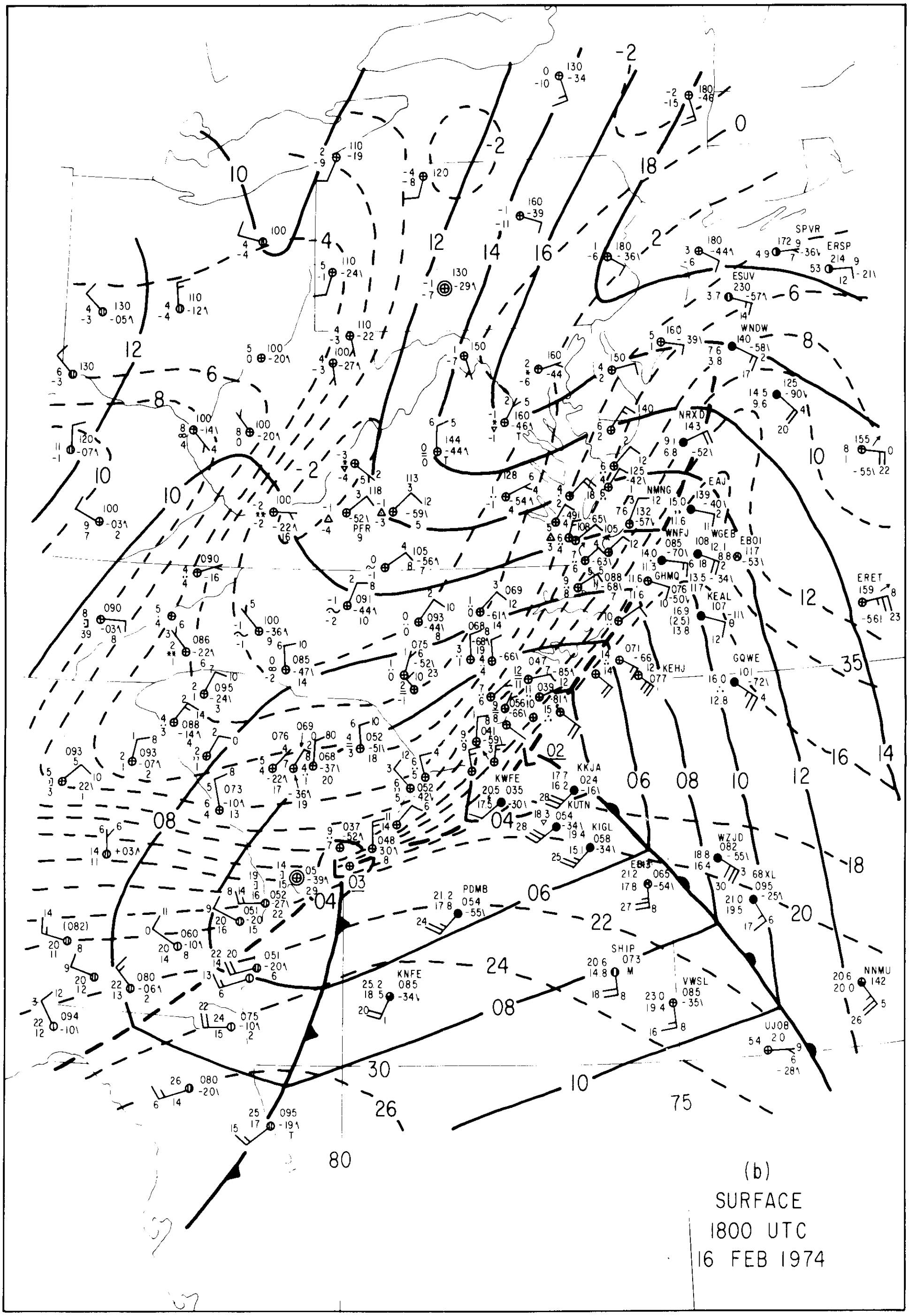

Fig. 2. (cont'd).

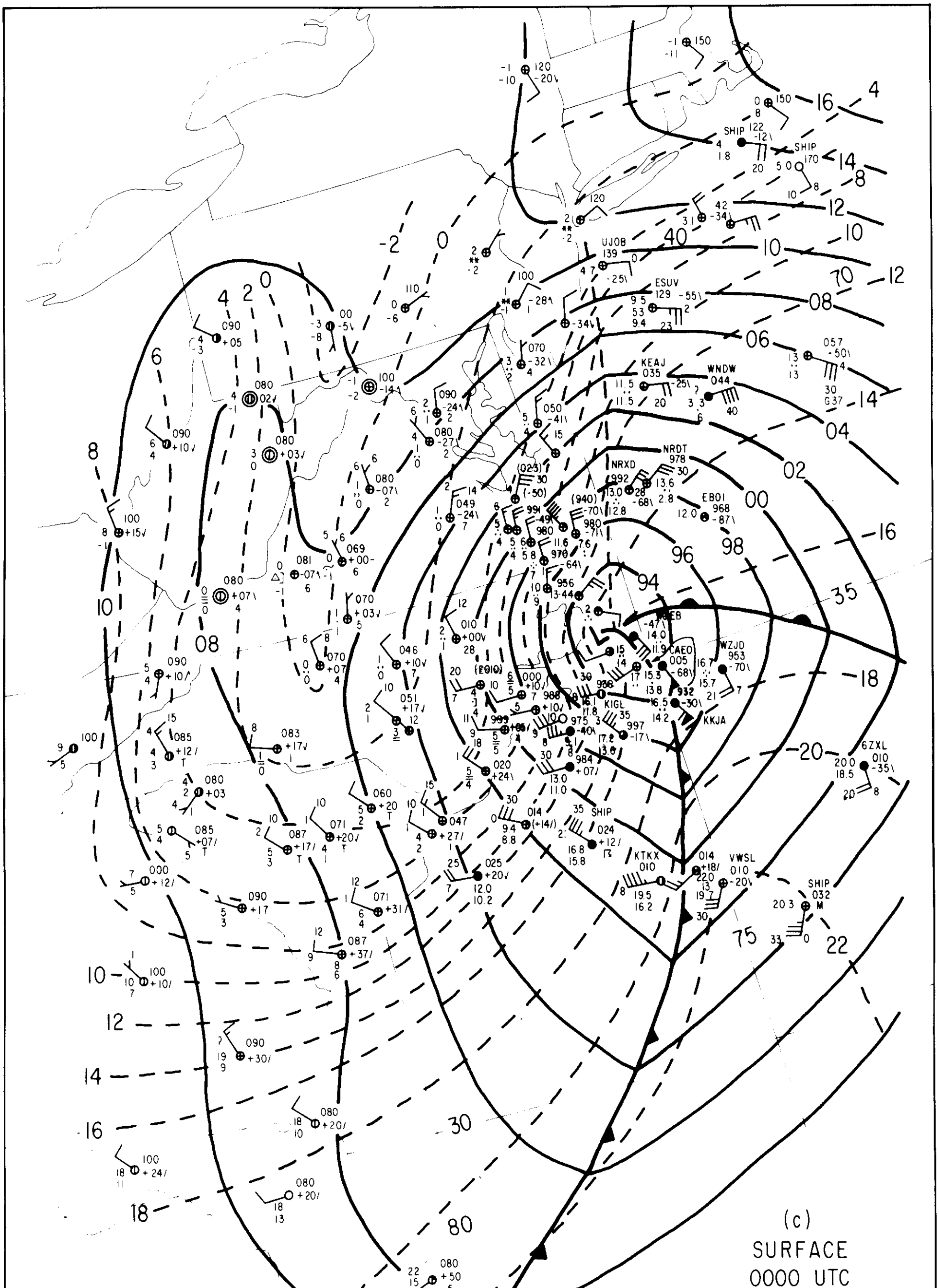

Fig. 2. (cont'd).

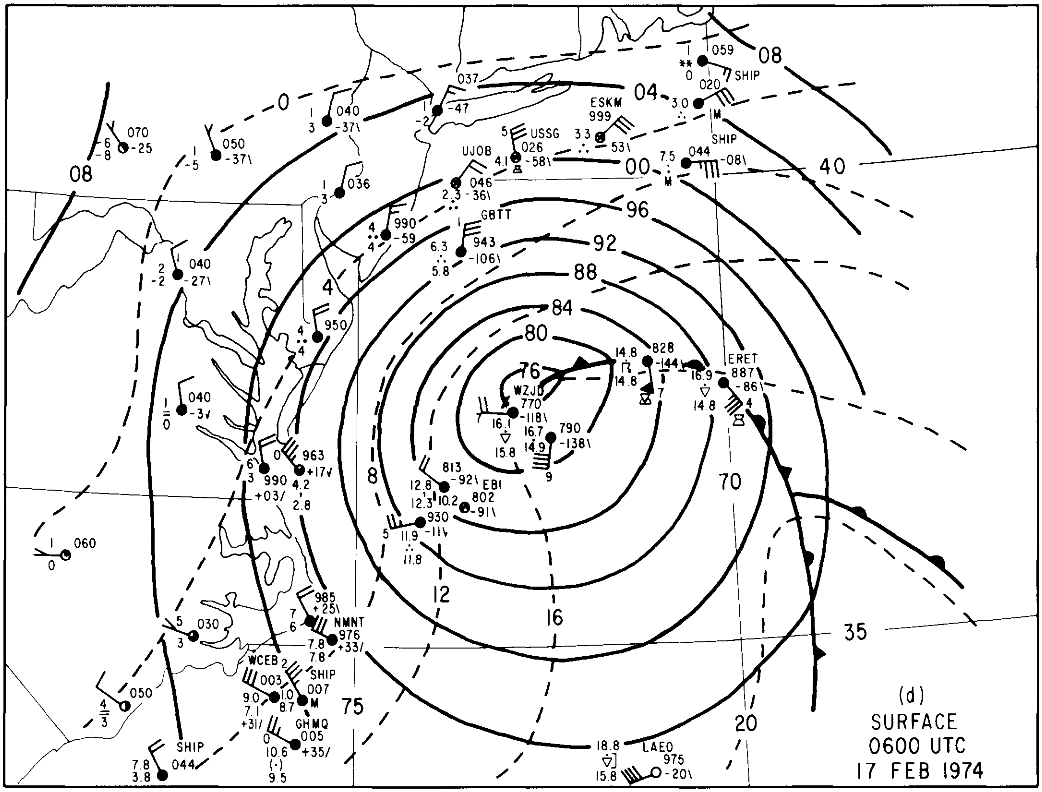

Fig. 2. (cont'd).

of the westerlies with one axis of the jet branching eastward across central Florida and a second branch forming farther north between 35–40° N.

A series of 850 mb, 500 mb, and 300 mb analyses for 1200 UTC 16 February and 0000 UTC 17 February are shown in Figs. 3a–f. The incipient cyclogenetic environment at 1200 UTC 16 February features the two aforementioned short wave disturbances with the southern short wave the most prominent with a 50–60 m s^{-1} wind maximum in the base of the 300 mb trough (Fig. 3c) over the southeastern United States. A second, and weaker, trough is positioned over the Great Lakes upstream of a short wave ridge over New England. Downstream a confluent jet entrance region is situated from Quebec to Nova Scotia at 500 mb and 300 mb (Figs. 3b, c) with maximum 300 mb wind speeds in excess of 60 m s^{-1}. This upper-level flow pattern, in which a short wave trough in the southern branch of the westerlies approaches a confluent jet entrance region, has been shown to be very favorable for cyclogenesis (see, e.g., Uccellini and Kocin, 1987; Bell and Bosart, 1988; Bell and Bosart, 1989; Uccellini, 1990). Note also that there is good warm air advection at 850 mb (Fig. 3a) along the Atlantic coast extending northward toward the eastern Great Lakes and Quebec and the right entrance of the aformentioned confluent 300 mb jet. The cyclogenetic region along the Atlantic coast (Fig. 2a) is situated on the cyclonic shear side of the southern jet (forward side of the progressive 500 mb trough) and to the southwest of the anticyclonic shear side of the downstream confluent 300 mb jet.

By 0000 UTC 17 February the rapidly intensifying surface cyclone (Fig. 2c) is positioned near the apex of the thermal wave of the prominent 500 mb southern short wave trough. The northeastward movement of the southern trough is associated with a strengthening of the downstream confluent

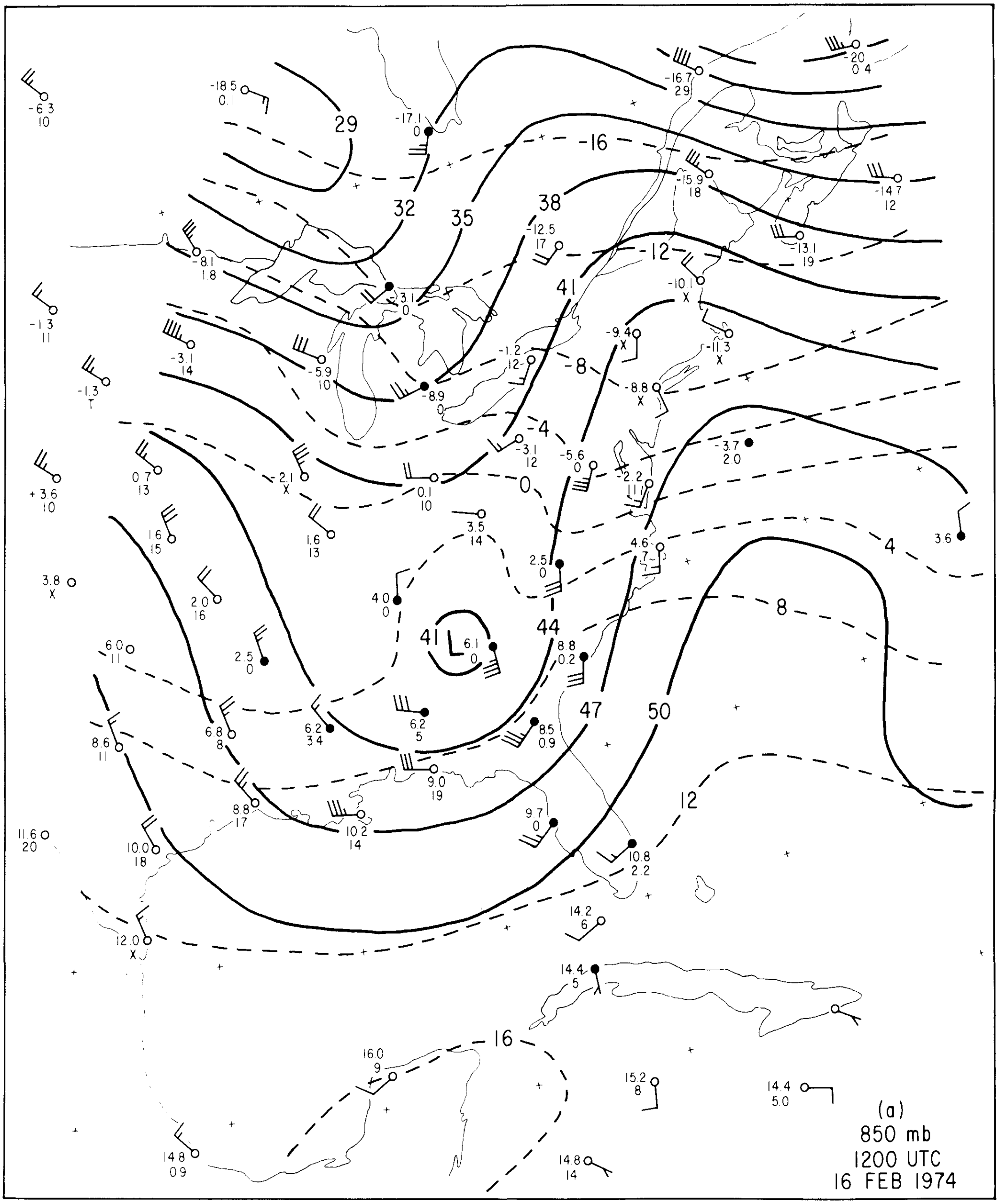

Fig. 3. Upper air sectional maps for 850 mb, 500 mb, and 300 mb at 1200 UTC 16 February 1974 (0000 UTC 17 February 1974) in panels (a, b, c) (panels (d, e, f)), respectively. Plotted winds are as in Fig. 2. Temperature and dew point temperature plotted to the nearest 0.1°C. Solid station circles denote a temperature-dew point temperature difference of <5°C, corresponding to an approximate relative humidity of 70%. Solid contours represent geopotential heights analyzed every 3 dam, 6 dam, and 12 dam at 850 mb, 500 mb, and 300 mb, respectively. Dashed lines denote isotherms analyzed every 4°C.

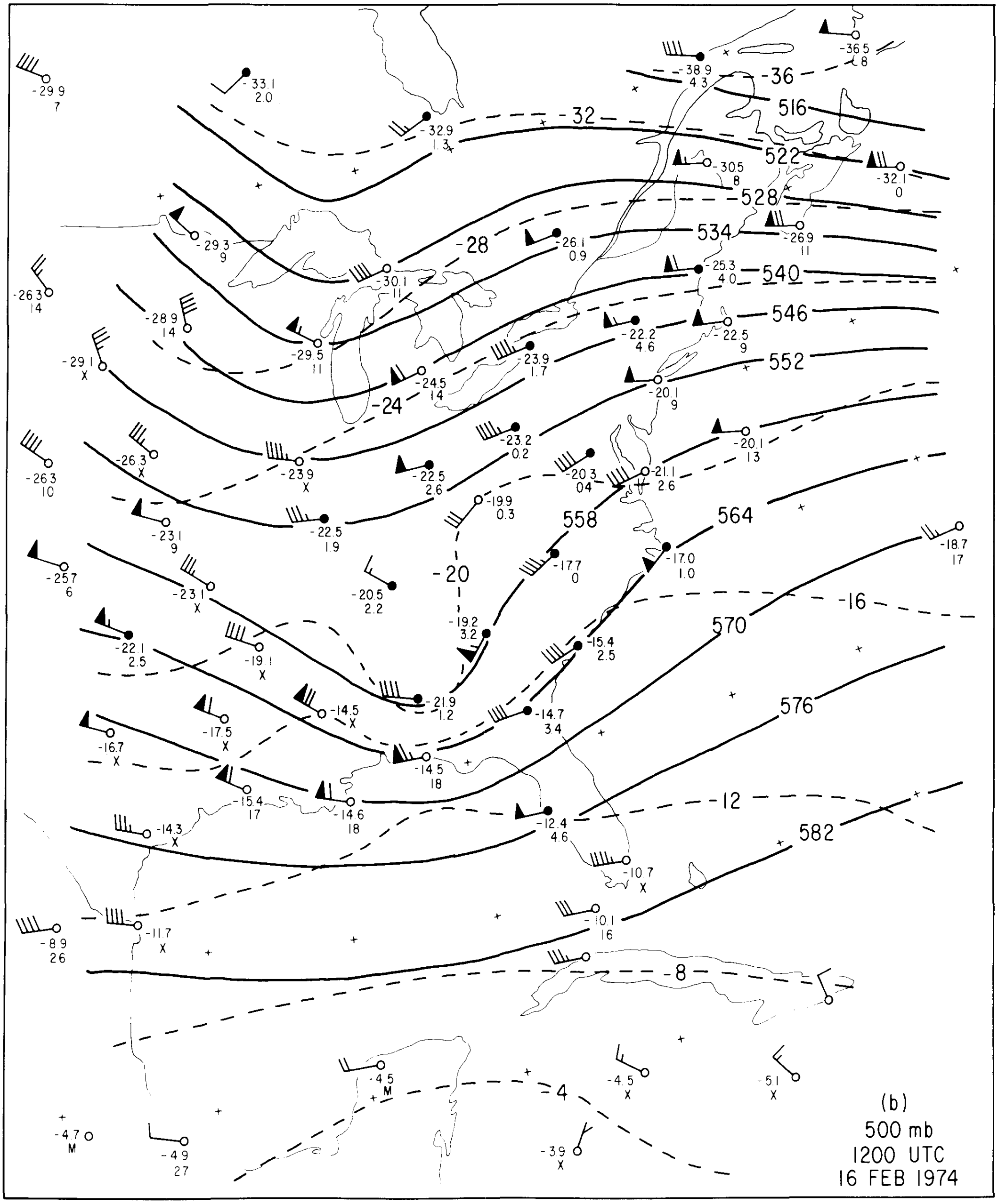
(b)
500 mb
1200 UTC
16 FEB 1974
516
522
528
534
540
546
552
558
564
570
576
582
-36
-32
-28
-24
-20
-16
-12
-8
-4

Fig. 3. (cont'd).

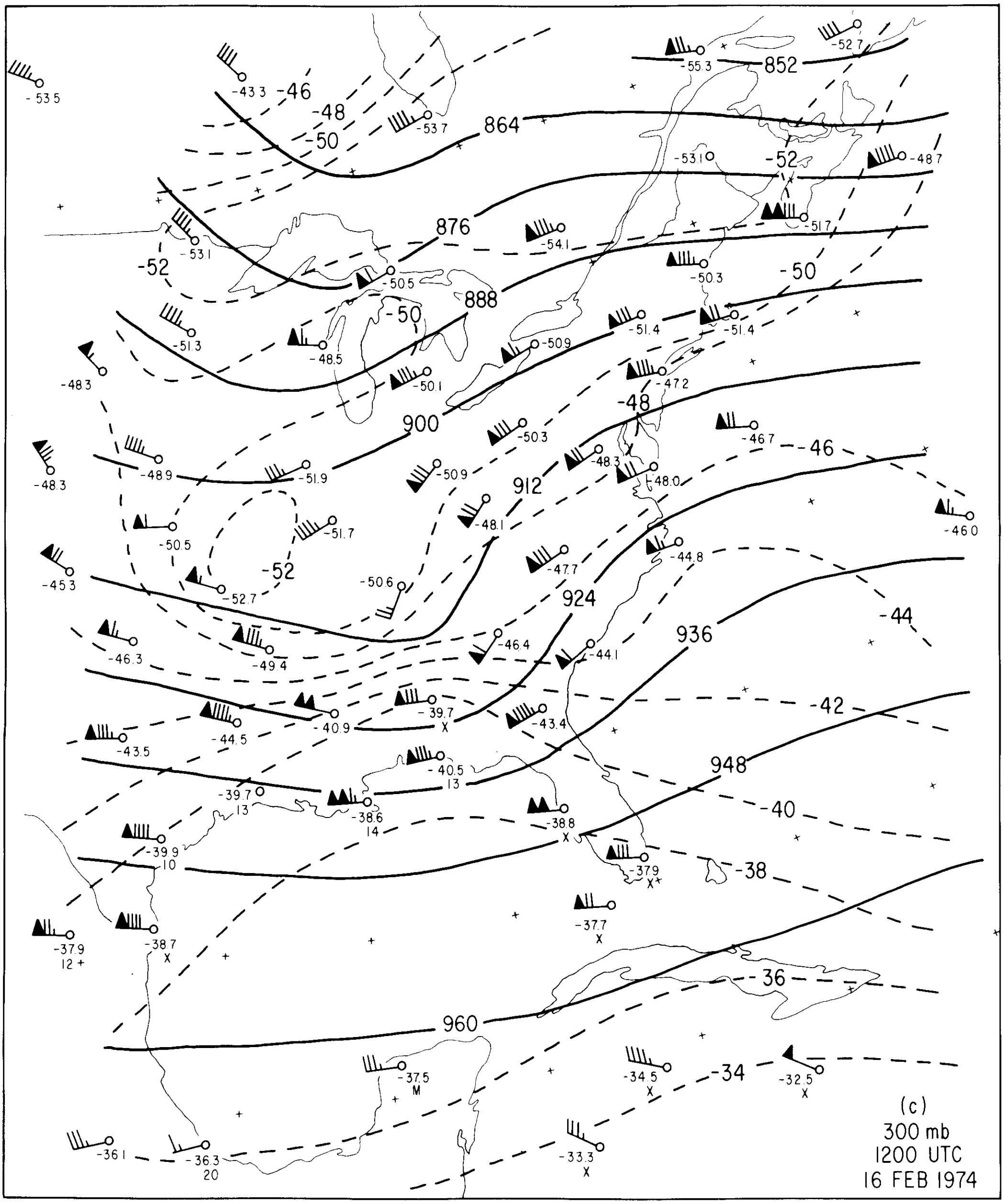
(c)
300 mb
1200 UTC
16 FEB 1974
852
864
876
888
900
912
924
936
948
960
-34
-36
-38
-40
-42
-44
-46
-48
-50
-52

Fig. 3. (cont'd).

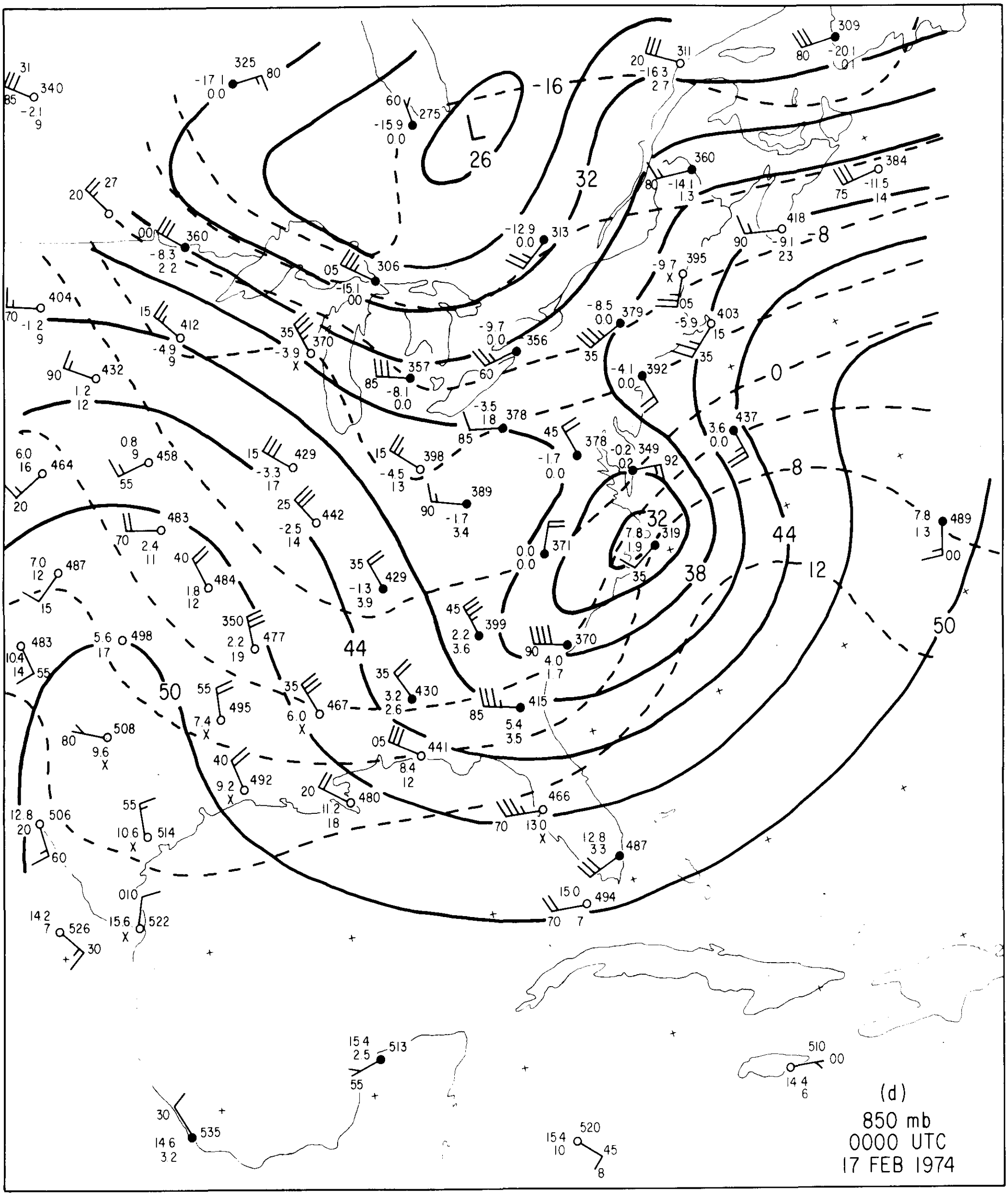

Fig. 3. (cont'd).

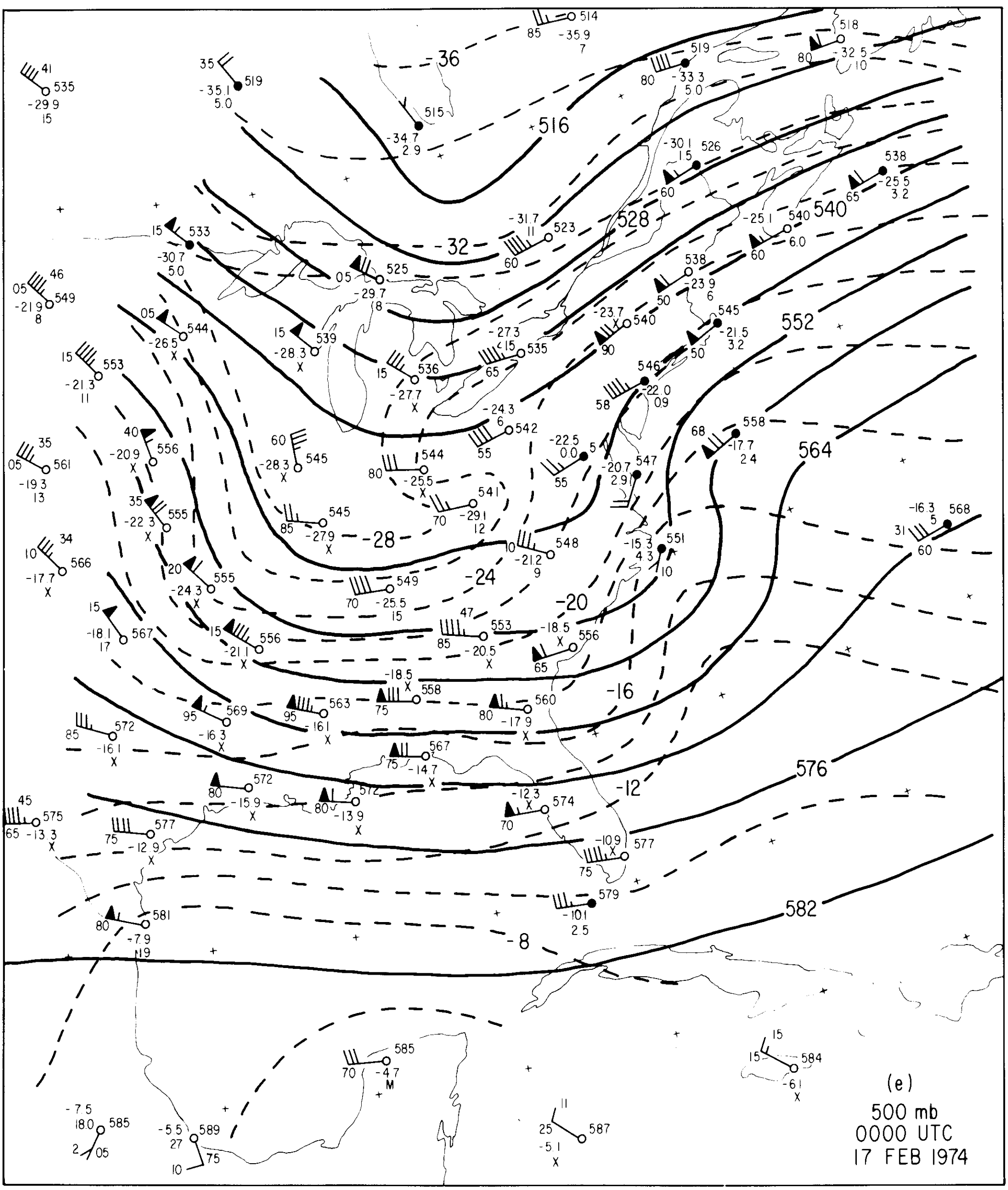
-36
516
-32
528
540
552
-28
-24
-20
564
-16
576
-12
582
-8
(e)
500 mb
0000 UTC
17 FEB 1974

Fig. 3. (cont'd).

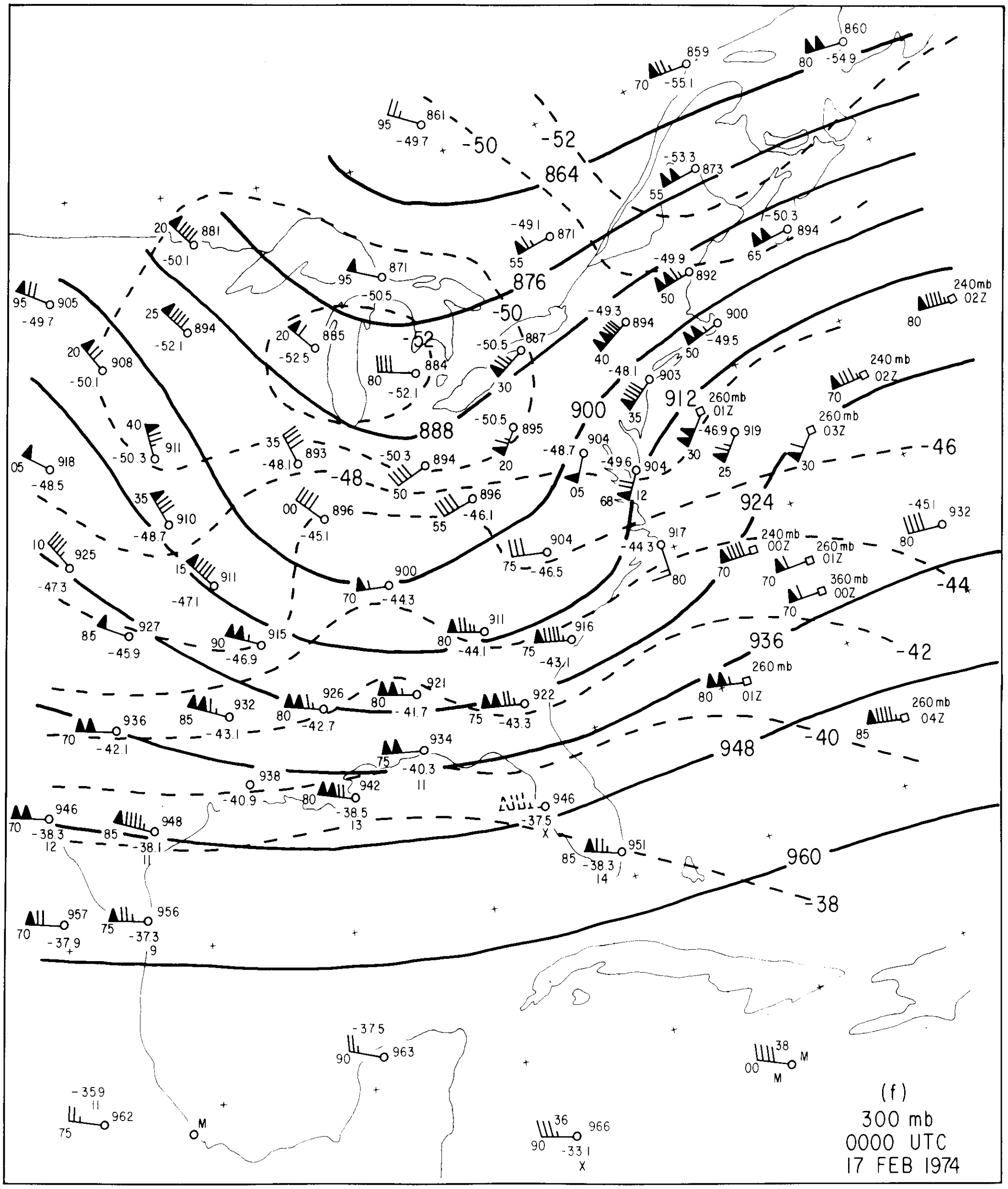

Fig. 3. (cont'd).

northern jet where the 300 mb wind speed maximum reaches almost 70 m s^{-1} over the northeastern United States. As the distance between the upstream and downstream jets decreases the intensifying surface and 850 mb cyclone centers (Figs. 2c, 3d) become situated in the favored region for estimated deep ascent (see section 3c) between them where the upward increase of cyclonic vorticity advection is also estimated to maximize. Note also the region of very weak southerly flow of ($<$5–10 m s^{-1}) at 500 mb and 300 mb (near HAT) and 850 mb warm air advection over coastal areas between the two strengthening jet streaks where deep tropospheric ascent is estimated to maximize. Warm air advection at 850 mb (Fig. 3d) to the north of the cyclone is also seen to lie over the region of the inverted trough in the coastal waters that marks the northward-developing coastal front seen in Figs. 2b, c.

A summary of the reconfiguration of the 300 mb geopotential field for the 36 h period ending 0000 UTC 17 February obtained by graphical subtraction of the corresponding 300 mb analyses is presented in Fig. 4. The dominant feature on the map is the rising heights (maximum of 30 dam) centered over New England and southeastern Canada. The height fall area to the southwest has one lobe along the Atlantic coast in the vicinity of the developing surface cyclone. A separate height fall center over the lower and central Mississippi Valley is associated with a third short wave trough (seen just entering the western domain of the 300 mb map east of the central Rockies in Fig. 3c) deepening into the longer wave trough position. This third trough plays an important role in cyclone development as it appears to act as a catalyst for discontinuous retrogression of the larger scale southern trough. The resulting amplification of the downstream ridge along the North Atlantic coast on the anticyclonic shear side of the persistent confluent flow pattern favors increasing southerly flow poleward of the eastern lobe of the aforementioned height fall center as is observed at 0000 UTC 17 February. The observed 36 h height change pattern in Fig. 4 is also consistent with strengthening northern and southern jet streaks as shown with the rapidly intensifying surface cyclone situated poleward (equatorward) of the exit (entrance) region of the southern (northern) jet.

The warm air advection region is also charac-

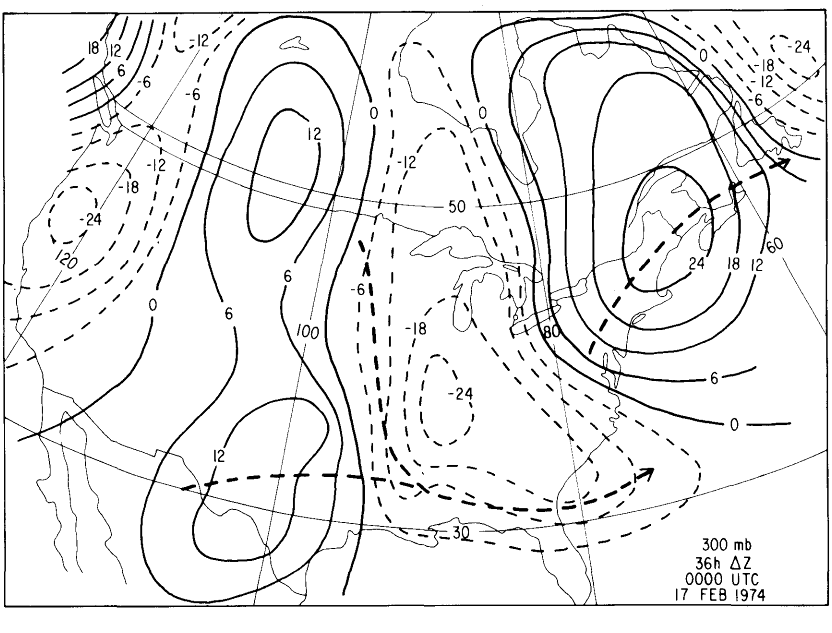

Fig. 4. 36 h 300 mb geopotential height change (contours every 6 dam) ending 0000 UTC 17 February 1974. Solid (dashed) contours denote height rises (falls) with the zero change contour shown heavy solid. Positions of the principal jet streaks at 0000 UTC 17 February are shown by the bold dotted lines.

terized by a deep layer of quasi-moist neutrality as can be seen for the soundings from ocean weather ship Hotel (4YH, 38° N, 71° W) and HAT at 0000 UTC 17 February shown in Fig. 5. Given the existence of deep, quasi-zero moist static stability implied by these soundings and the favorable position of this air mass between the two jet streaks (Fig. 4), we estimate that vigorous ascent (confirmed from the pattern of Q-vector convergence in the next section) is likely in the immediate vicinity of the intensifying surface cyclone. Additionally, embedded deep moist convection is possible along the southeastern flank of the cyclone where warm moist air that was previously in residence over the Gulf Stream (Fig. 1) is swept northwestward and ingested into the updraft region of the cyclone. For example, if we assume saturated air with a surface temperature of 18°C approaches the cyclone center a surface-based lifted index of -3.3 is

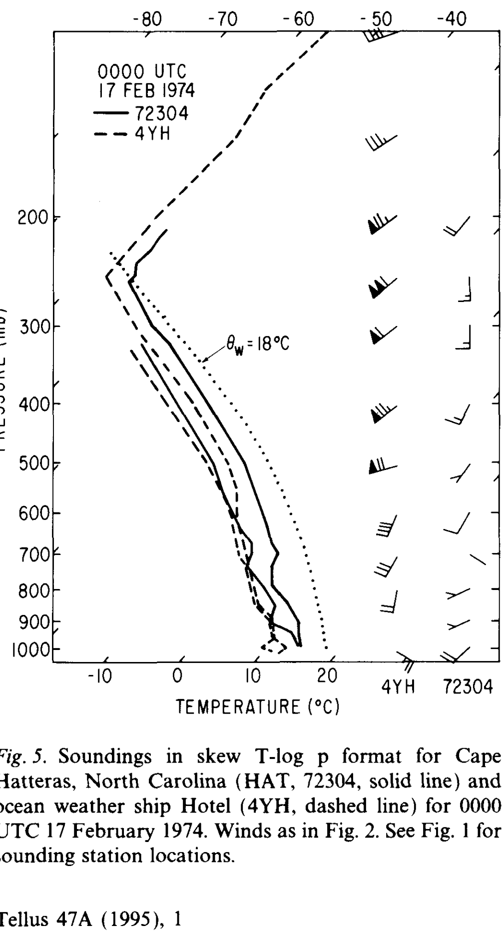

Fig. 5. Soundings in skew T-log p format for Cape Hatteras, North Carolina (HAT, 72304, solid line) and ocean weather ship Hotel (4YH, dashed line) for 0000 UTC 17 February 1974. Winds as in Fig. 2. See Fig. 1 for sounding station locations.

estimated based upon the observed HAT 500 mb temperature of -15.3°C. The estimated mid-level buoyancy of 3–4°C is based upon optimal conditions following the ideas of simple parcel dynamics. Note that from Figs. 2b, c there are no reports of thunderstorms along the coast as the cyclone begins to deepen rapidly. However, at 0600 UTC 17 February (Fig. 2d) a ship east of the cyclone center does report a thunderstorm in progress. Observations from the coastal radars of the United States National Weather Service (not shown), however, reveal the existence of embedded convection within the general precipitation shield in the coastal waters between 1800 UTC 16 February and 0000 UTC 17 February. Tracton (1973) showed that convection near the cyclone center was a characteristic of incipient rapid cyclogenesis in many cases and that the operational numerical prediction models then in use frequently underestimated the rate of cyclogenesis when deep convection was present near the cyclone center.

3.3. *Q vector forcing at 0000 UTC 17 February*

We show in Fig. 6 the convergence of the Q-vector, $\nabla \cdot \boldsymbol{Q}$, after Hoskins et al. (1978) and Hoskins and Pedder (1980) and the geostrophic frontogenesis function, F_g (divided by $|\nabla\theta|$ to be expressed in standard units) at 850 mb, 500 mb, and 300 mb for 0000 UTC 17 February in order to quantify some of our previous qualitative conclusions. Here Q and F_g are defined by (using conventional symbols):

$$\boldsymbol{Q} = \left\{ -\frac{R}{p}\frac{\partial \boldsymbol{V}_g}{\partial x} \cdot \nabla T_v, \; -\frac{R}{p}\frac{\partial \boldsymbol{V}_g}{\partial y} \cdot \nabla T_v \right\} \tag{1}$$

and

$$F_g \equiv \frac{d}{dt}|\nabla\theta|^2 = 2\left(\frac{p_0}{p}\right)^{R/c_p}\left(\frac{p}{R}\right)\boldsymbol{Q}\cdot\nabla\theta. \tag{2}$$

As shown initially by Hoskins et al. (1978) the Q-vector has the property that it can be related to the quasi-geostrophic vertical motion according to:

$$\sigma\nabla^2\omega + f_0^2\frac{\partial^2\omega}{\partial p^2} = -2\nabla\cdot\boldsymbol{Q} \tag{3}$$

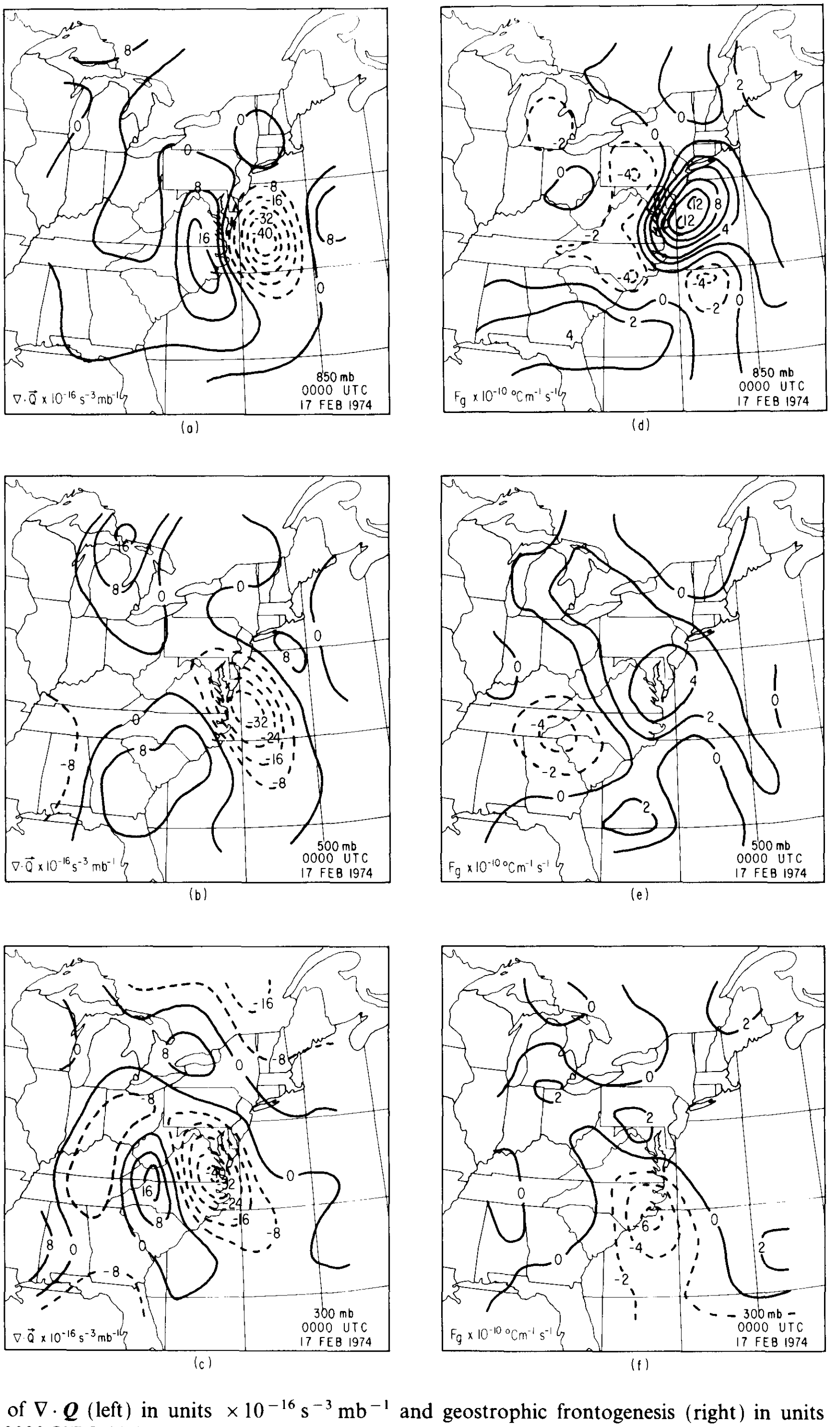

Fig. 6. Field of $\nabla \cdot \boldsymbol{Q}$ (left) in units $\times 10^{-16}$ s^{-3} mb^{-1} and geostrophic frontogenesis (right) in units $\times 10^{-10}$ °C m^{-1} s^{-1} for 0000 UTC 17 February 1974 for 850 mb (a, d), 500 mb (b, e), and 300 mb (c, f). Positive and negative values denoted by solid and dashed contours respectively.

where, σ, the static stability computed as:

$$\sigma = -\frac{R}{p}\left(\frac{p}{p_0}\right)^{R/c_p}\frac{\partial\theta}{\partial p}. \tag{4}$$

According to (3) areas of convergence (divergence) of $\boldsymbol{Q}$ are associated with quasi-geostrophic ascent (descent) with the $\boldsymbol{Q}$-vector pointing in the direction of the lower branch of the quasi-geostrophic secondary circulation. Hoskins and Pedder (1980) also observed that F_g would be frontogenetical (frontolytical) where $\boldsymbol{Q}$ was directed toward higher (lower) potential temperatures on an isobaric surface. Equivalently, a normalized version of (2) can be computed from Miller's (1948) frontogenesis equation (equivalent to dividing (2) by the magnitude of the horizontal potential temperature gradient) with only the horizontal confluence terms retained and the horizontal wind components replaced by their geostrophic equivalents, and this calculation is what appears in Figs. 6d–f.

We chose to display $\nabla \cdot \boldsymbol{Q}$ in Fig. 6 instead of the full quasi-geostrophic vertical motion because of the limited vertical resolution and relatively small horizontal domain of our manually analyzed and digitized geopotential height and temperature data. Despite these limitations it is apparent from Fig. 6 that the fields of $\nabla \cdot \boldsymbol{Q}$ are quite robust in the vicinity of the rapidly intensifying cyclone center at 0000 UTC 17 February. Generally, the region of $\nabla \cdot \boldsymbol{Q} < 0$ is vertically consistent and slopes northwestward with height, implying deep ascent over and just ahead of the surface cyclone center. Comparison with Figs. 3–4 clearly shows that the region of $\nabla \cdot \boldsymbol{Q} < 0$ is situated in the estimated favorable ascent zone between the northern and southern jet streaks. Equally impressive, the magnitude of the $\nabla \cdot \boldsymbol{Q} < 0$ region at 850 mb (Fig. 6a) is just as large as it is at 500 mb and 300 mb (Figs. 6b, c), further indicative of estimated deep tropospheric ascent discussed previously. Further support for this statement is seen in the pattern of quasi-geostrophic frontogenesis given by F_g in Figs. 6d–f. Geostrophic frontogenesis maximizes at 850 mb (Fig. 6d) along the coast to the northeast of the cyclone center where coastal frontogenesis is occurring along the inverted trough shown in Fig. 2c. The geostrophic frontogenesis weakens upward through 500 mb (Fig. 6e) while extending northwestward across Pennsylvania with a separate maximum identified at 300 mb (Fig. 6f) in the entrance region of the northern jet (Fig. 3f).

Note also that the northwestward tilt of the region of $\nabla \cdot \boldsymbol{Q} < 0$ across the Delmarva peninsula into Pennsyslvania at 500 mb and 300 mb implies that deep ascent can also be found to the northwest of the cyclone center to the immediate southwest of the northern jet. The existence of this implied ascent is confirmed by the presence of widespread reported stratiform precipitation to the northwest of the cyclone center at 0000 UTC 17 February shown in Fig. 2c. As discussed by Bell and Bosart (1989) for other cases of eastern North American cyclogenesis, and applicable to this case, the $\boldsymbol{Q}$-vector approach can be used to reconcile quasi-geostrophic vertical motion patterns associated with differential vorticity advection and thermal advection with the vertical motions postulated to exist in association with jet-induced vertical circulations as originally described by Sutcliffe and Forsdyke (1950), Beebe and Bates (1955) and quantified by Uccellini and Johnson (1979). The configuration of the 300 mb jets shown in Fig. 3f (and summarized in Fig. 4) favors estimated cyclonic and anticyclonic vorticity maxima on the cyclonic and anticyclonic shear sides of the respective jet streaks such that cyclonic vorticity advection (the dominant deepening mechanism in the "traditional" form of the omega equation; Bluestein, 1992 and Holton, 1992) would be maximized between the two jet streaks where surface development is occurring.

Kocin and Uccellini (1990, their Fig. 21) have interpreted this configuration of dual jet streaks as favorable to explosive cyclogenesis along the east coast of North America because of the superposition of the ascending branches of both jet streaks over the favored surface development region. However, as noted here and in Bell and Bosart (1989) such a superposition can be manifest as a single region of concentrated Q-vector induced ascent at the time of explosive surface development. (We also state without proof that the above interpretation is also consistent with "potential vorticity thinking", Hoskins et al., 1985, in that relatively low potential temperatures on the tropopause poleward of the southern jet streak and relatively high potential temperatures on the tropopause equatorward of the northern jet streak would favor cold advection along the tropopause and induced cyclonic circulation below over the developing surface cyclone center.)

3.4. *Surface development*

The purpose of this section is to document the surface development at 1800 UTC 16 February and 0000 UTC 17 February as rapid intensification commenced. All calculations were derived from the previously described manually analyzed maps of mean sea level pressure, temperature, dew point temperature and wind speed and direction that were gridded on a one degree latitude-longitude mesh. Centered differences were used for all calculations.

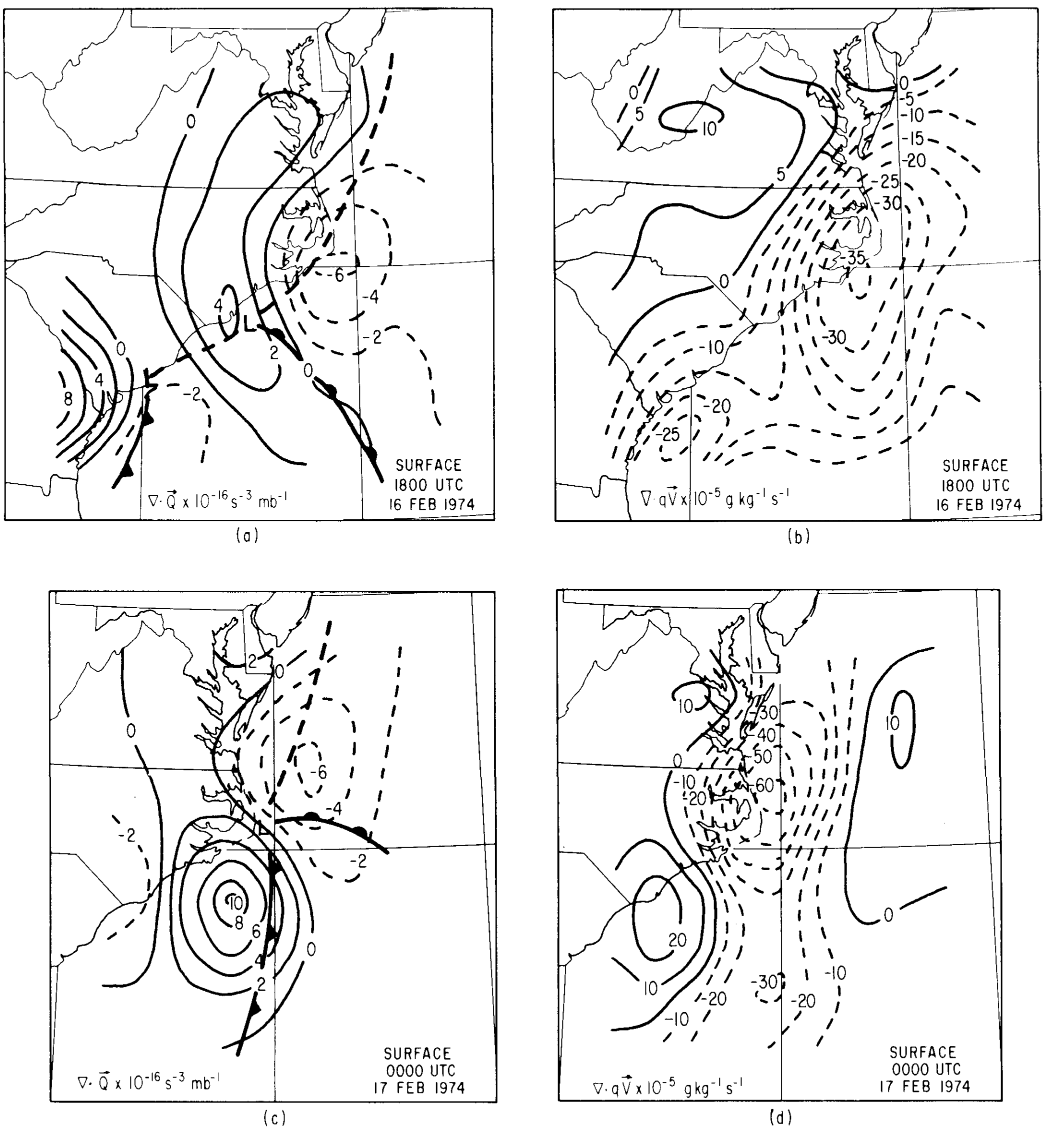

Fig. 7. Field of $\nabla \cdot \boldsymbol{Q}$ (units as in Fig. 6) at the surface for (a) 1800 UTC 16 February 1974 and (c) 0000 UTC 17 February 1974. Corresponding field of $\nabla \cdot q\boldsymbol{V}$ (in units $\times 10^{-5}$ g kg^{-1} s^{-1}) shown in (b) and (d). Positive and negative values are denoted by solid and dashed contours, respectively.

(*i*) *Moisture and* $\boldsymbol{Q}$*-vector convergence*

The maps of $\nabla \cdot \boldsymbol{Q}$ (computed from surface geostrophic winds derived from the manually-analyzed sea level pressure fields) reveal that convergence is maximized in general downstream of the surface cyclone position at both time periods (Figs. 7a, c) with some suggestion for a tongue of $\nabla \cdot \boldsymbol{Q} < 0$ extending northward along the developing coastal front. Comparison of Figs. 2b and 7a support the idea that secondary sea level cyclogenesis is favored progressively downstream along the coastal baroclinic zone as the primary cyclone weakens to the west of the Appalachians. This interpretation is also supported by the moisture convergence maps using the observed winds ($\nabla \cdot q\boldsymbol{V}$, Figs. 7b, d) which show a near doubling of the quasi-stationary moisture con-

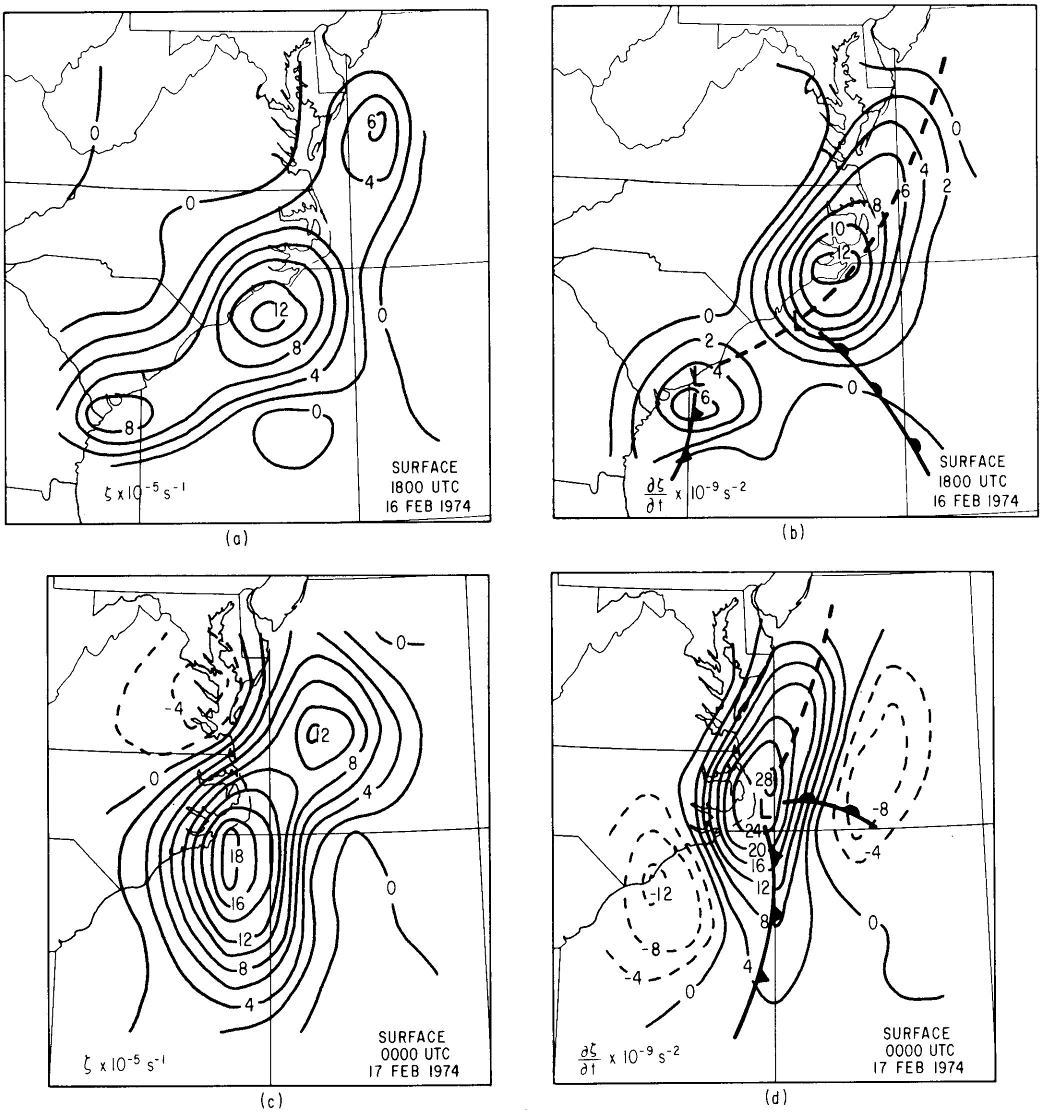

Fig. 8. As in Fig. 7 except for the relative vorticity (a, c in units $\times 10^{-5}\ s^{-1}$) and the relative vorticity tendency (b, d in units $\times 10^{-9}\ s^{-2}$). Surface frontal positions as indicated.

vergence maximum located over extreme eastern North Carolina and the adjacent coastal waters in the 6 h ending 0000 UTC 17 February.

(ii) Vorticity

Our vorticity analysis is based upon the observed winds and the following form of the vorticity equation applicable at the surface where the vertical motion is assumed to vanish and friction is ignored:

$$\frac{\partial \zeta}{\partial t} = -\boldsymbol{V} \cdot \nabla(\zeta + f) - (\zeta + f)\, \nabla \cdot \boldsymbol{V}, \tag{5}$$

where ζ and f represent the relative vorticity and Coriolis parameter, respectively, and the other

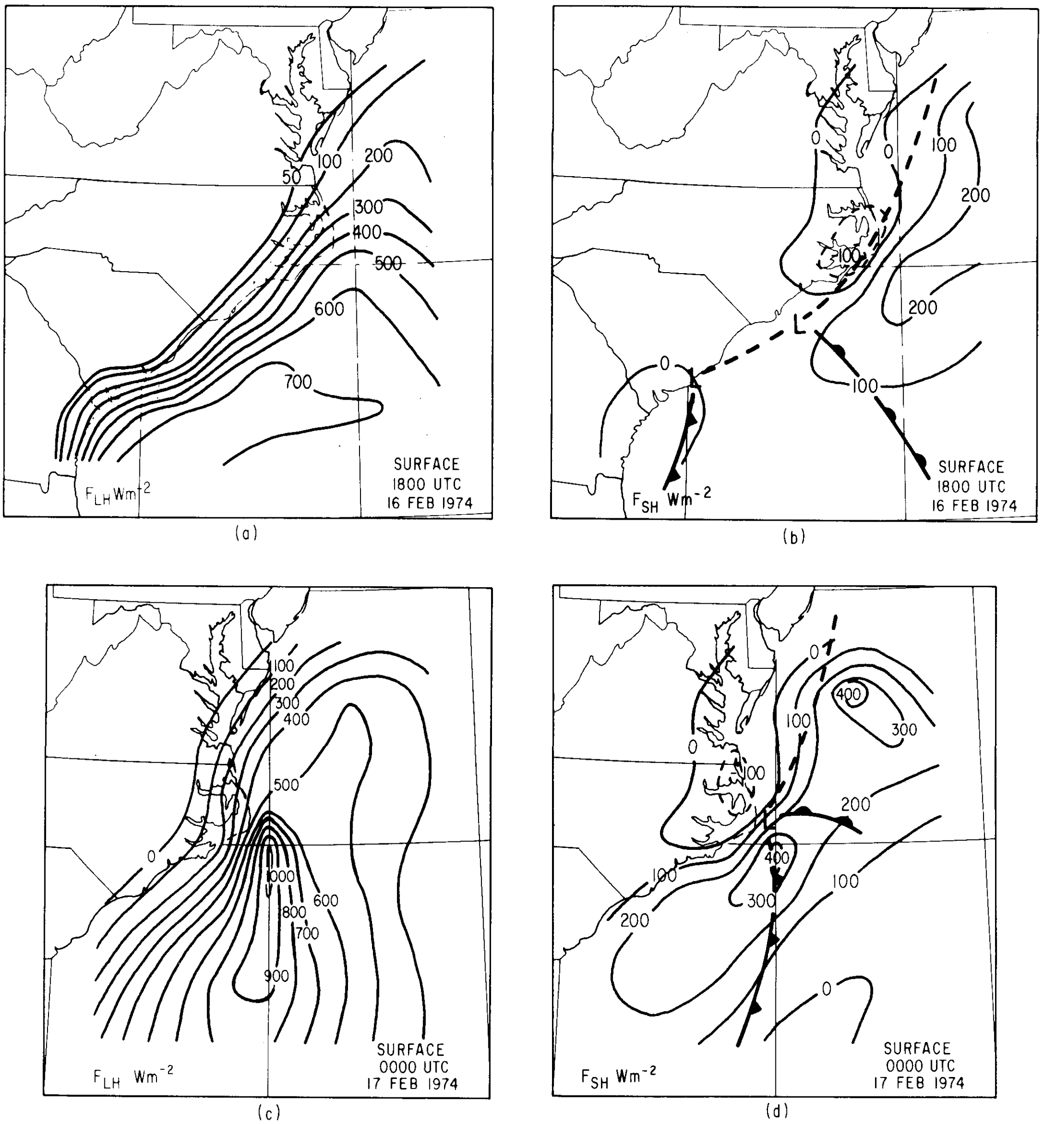

Fig. 9. As in Fig. 7 except for surface latent heat (a, c in W m^{-2}) and sensible heat fluxes (b, d in units of W m^{-2}). Surface frontal positions as indicated.

terms have their using meaning. The vorticity maps (Figs. 8a, c) reveal that cyclonic relative vorticity maximizes along the coastal baroclinic zone while extending northward along the developing coastal front and inverted trough. Twin maxima along the Carolina coast at 1800 UTC 16 February mark the circulation centers identified on the surface map for the same time (Fig. 2b). However, comparison with the vorticity tendency map for the same time (Fig. 8b) suggests that the northern vorticity center along the Carolina coast will become the principal center (also confirmed from the $\nabla \cdot \boldsymbol{Q}$ and $\nabla \cdot q\boldsymbol{V}$ maps in Fig. 7). Note that the vorticity tendency more than doubles over

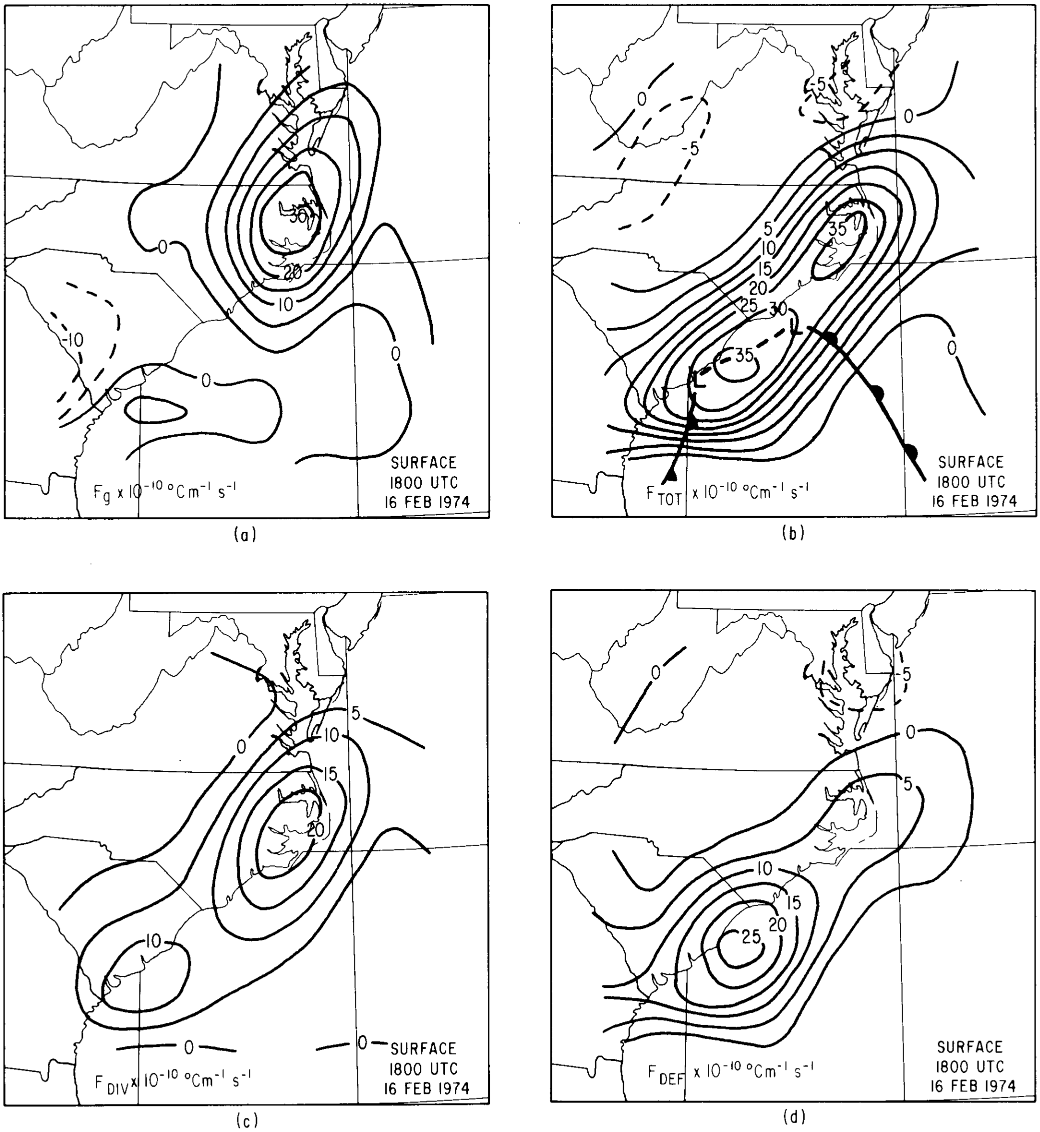

Fig. 10. Geostrophic frontogenesis (a), total observed wind frontogenesis (b), contribution of divergence to the total observed wind frontogenesis (c), and contribution of the deformation to the total observed wind frontogenesis (d) for 1800 UTC 16 February 1974. Units $\times 10^{-10}$ °C m^{-1} s^{-1} with solid and dashed contours denoting frontogenesis and frontolysis, respectively. Surface frontal positions as indicated.

the next 6 h with a computed peak value of $30 \times 10^{-9}\,s^{-2}$ at 0000 UTC 17 February just to the north of the cyclone center. This maxima, elongated north-northeastward along the offshore coastal front and inverted trough, is dominated by the convergence term in (5).

(iii) Surface sensible and latent heat fluxes

The surface sensible and latent heat fluxes computed from the standard bulk aerodynamic formula with a constant exchange coefficient of 1.5×10^{-3} are displayed in Fig. 9. At 1800 UTC 16

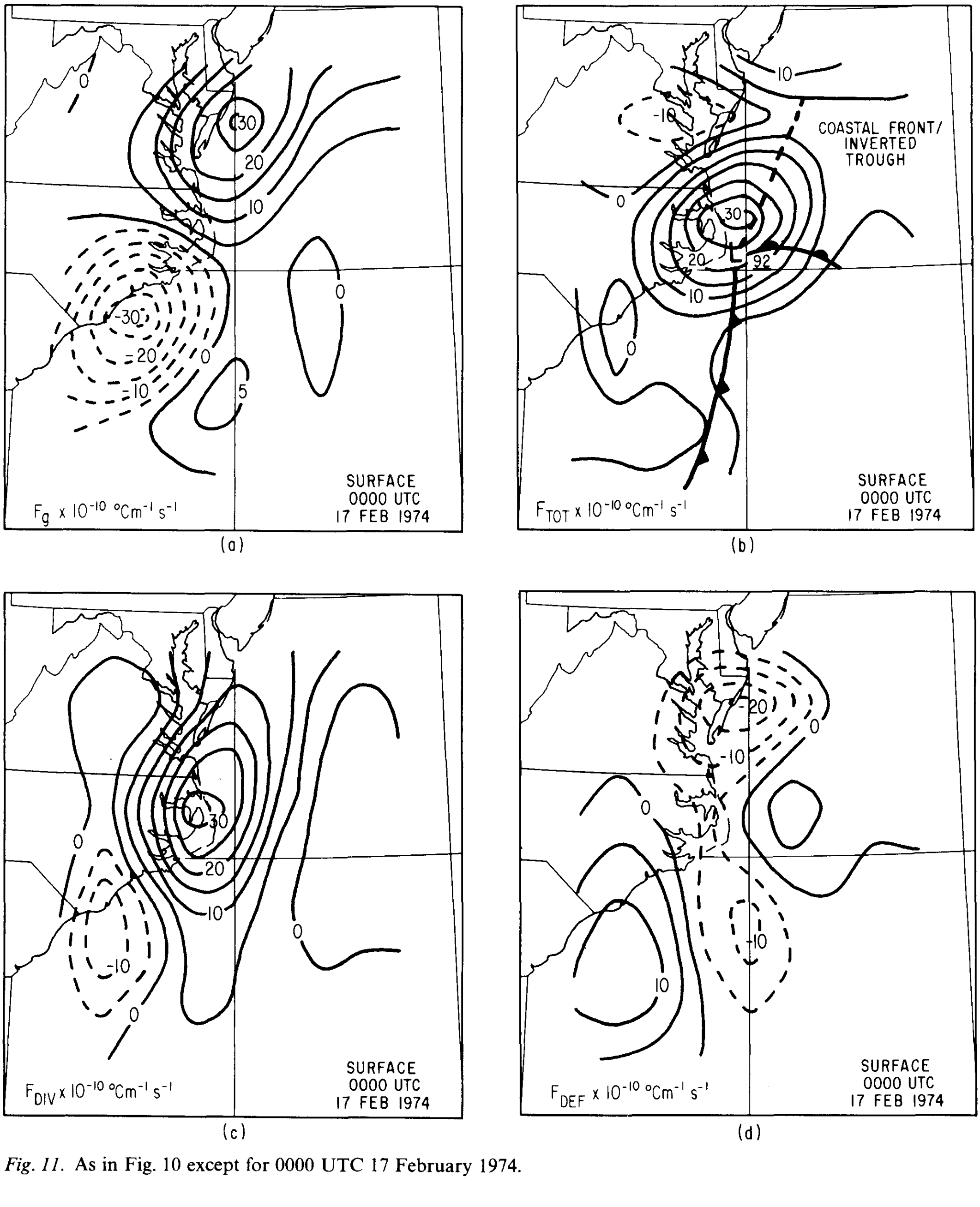

Fig. 11. As in Fig. 10 except for 0000 UTC 17 February 1974.

February surface sensible heat fluxes in excess of 200 W m^{-2} (Fig. 9b) maximize along the edge of the Gulf Stream in the coastal waters to the northeast of the developing cyclone. These heat fluxes almost double in the next 6 h (Fig. 9d), reaching a peak value of 400 W m^{-2} in the coastal front/inverted trough region northeast of the cyclone center and immediately to the south of the cyclone center as colder air in the wake of the cyclone begins to wrap cyclonically around the disturbance over the warmer oceanic waters. The latent heat fluxes average double to triple the sensible heat fluxes at both times (Figs. 9a, c). During the incipient rapid cyclogenesis underway at 1800 UTC 16 February the maximum latent heat flux lies along the southeastern flank of the developing cyclone with a prominent nose extending northward along the offshore coastal front. Especially impressive is the narrow tongue of large latent and sensible heat fluxes ($\sim$1000 W m^{-2} and 400 W m^{-2}, respectively) centered near 35° N and 75° W at 0000 UTC 17 February. Comparison of Figs. 9c, d with Fig. 2c shows that this tongue of high sensible and latent heat flux corresponds to the narrow southerly jet just to the south of the cyclone center immediately in advance of the surface cold front.

(iv) Surface frontogenesis

The distribution of surface geostrophic and observed wind frontogenesis is mapped in Figs. 10, 11 for 1800 UTC 16 February and 0000 UTC 17 February, respectively. The observed wind frontogenesis is computed from the Miller (1948) frontogenesis equation with the diabatic heating and twisting terms ignored as follows:

$$\frac{\mathrm{d}}{\mathrm{d}t}|\nabla\theta| = \frac{1}{|\nabla\theta|}\left\{\frac{\partial\theta}{\partial x}\left[-\frac{\partial u}{\partial x}\frac{\partial\theta}{\partial x}-\frac{\partial v}{\partial x}\frac{\partial\theta}{\partial y}\right]\right.$$
$$\left.+\frac{\partial\theta}{\partial y}\left[-\frac{\partial u}{\partial y}\frac{\partial\theta}{\partial x}-\frac{\partial v}{\partial y}\frac{\partial\theta}{\partial y}\right]\right\}. \tag{6}$$

Here, θ is the potential temperature and u and v represent the zonal and meridional components of the wind, positive eastward and northward, respectively.

Note that (6) is numerically equivalent to a normalized version of (2) with the observed wind components replacing the geostrophic wind components. Comparison of the geostrophic and observed wind frontogenesis at 1800 UTC 16 February (Figs. 10a, b) reveals that the observed wind frontogenesis maximum, while in agreement with the geostrophic maximum over extreme eastern North Carolina, is much more elongated along the coastal baroclinic zone. The maximum observed wind frontogenesis is dominated by the divergence term (Fig. 10c) and the deformation term (Fig. 10d) at the northern and southern ends of the coastal baroclinic zone, respectively. Comparison of Figs. 10c, d with Fig. 8b reveals the common role of horizontal convergence in producing cyclonic vorticity in the presence of a strengthening coastal baroclinic zone. A slight weakening of the observed wind frontogenesis tendency is seen by 0000 UTC 17 February (Fig. 11b) as the deformation term (Fig. 11d) begins to act in opposition to the divergence term (Fig. 11c) in the coastal waters. Note, however, that the geostrophic frontogenesis maximum at this time (Fig. 11a) lies to the north of the cyclone center along the offshore coastal front and inverted trough and is comparatively weak near the cyclone center. Our results indicate that surface frontogenesis processes by the ageostrophic wind cannot be ignored during incipient coastal cyclogenesis. This finding is consistent with results reported elsewhere by, e.g., Bosart (1975), Bosart and Lin (1984), Bosart (1984), and Keshishian and Bosart (1987).

4. Concluding discussion

This paper has described a case of explosive cyclogenesis along the east coast of North America from February 1974. A noteworthy aspect of the cyclone development included a deepening rate of 36 mb in 15 h as the cyclone tracked across the Gulf Stream boundary toward warmer water (including a warm Gulf Stream ring containing 24°C sea water). The Gulf Stream was situated farther northwest in January and February 1974 than normal with resultant +3 to +6°C SST anomalies in the 35–40° N and 70–75° W latitude-longitude rectangle across which the cyclone tracked. The case was selected because it provided a good example of cyclone development in response to the reorganization of the flow pattern aloft so as to favor the juxtaposition of separate jet streaks in the northern and southern branches of the westerlies along the Atlantic coast so that $\boldsymbol{Q}$-vector convergence would be maximized throughout the troposphere in the vicinity of the developing cyclone center. Analysis was limited to the incipient stage of explosive cyclogenesis in the coastal zone where coverage by conventional data platforms was unusually good.

The February 1974 cyclone developed in the coastal waters along the southeastern coast of the United States as a weak predecessor cyclone dissipated to the northwest along the western slopes of the Appalachian Mountains. Cyclogenesis commenced as a progressive short wave trough/jet streak system in the southern branch of the westerlies reached the coast. Rapid coastal intensification began as this trough approached a strengthening jet entrance region embedded in confluent flow in the northern branch of the westerlies over New England and the Canadian Maritimes. Discontinuous retrogression in the southern branch of the westerlies enabled the coastal trough aloft to lift northeastward in association with ridging and a strengthening of the downstream jet. An analysis of the field of $\nabla \cdot \boldsymbol{Q}$ at 0000 UTC 17 February (the time of most rapid surface cyclogenesis) revealed the existence of a concentrated area of tropospheric-deep $\nabla \cdot \boldsymbol{Q} < 0$ (and implied ascent) that tilted northwestward with height from near the cyclone center at 850 mb. This deep layer of $\nabla \cdot \boldsymbol{Q} < 0$ was situated between the poleward left exit region of the southern jet streak and the equatorward right entrance region of the northern jet streak, a region favorable for cyclogenesis as noted by Uccellini et al. (1985, 1987), Bell and Bosart (1988, 1989), Kocin and Uccellini (1990), and Uccellini (1990) in conjunction with other storms over eastern North America. As noted here, and in Bell and Bosart (1989), the interaction of the two jet streaks resulted in a wind pattern in the middle and upper troposphere that favored an estimated large area of cyclonic vorticity advection in the upper troposphere over the intensifying cyclone center. The dual ascending branches of the overlapping jet streak circulations, Kocin and Uccellini (1990; their Fig. 21), were manifest here as a single concentrated maximum of $\nabla \cdot \boldsymbol{Q} < 0$ and implied ascent. Accordingly, the "traditional" and $\boldsymbol{Q}$-vector forms of the omega equation (Bluestein, 1992; Holton, 1992) can be reconciled with vertical circulations associated with jet entrance and exit regions (see, e.g., Beebe and Bates, 1955; Uccellini and Johnson, 1979) to yield a coherent picture of incipient synoptic scale cyclogenesis at the level of quasi-geostrophic theory.

The development of the February 1974 cyclone was also qualitatively in accord with the climatologies of explosive cyclones (a.k.a. bombs) presented by Sanders and Gyakum (1980) and Roebber (1984). For example, Roebber's (1984) updated 6-year (1976–1982) climatology showed that explosive cyclone formation maximized in the coastal waters from extreme northern Florida to the Carolinas (his Fig. 5c) while the area of maximum 24-h deepening extended from $\sim$200 km northeast of extreme northeastern North Carolina to the southern tip of Nova Scotia (his Fig. 7c). The February 1974 cyclone formed in Roebber's favored region and deepened explosively at the southwestern end of his area of most rapid deepening. Comparison with the composite surface and upper air climatology of explosive Atlantic ocean cyclogenesis presented by Rogers and Bosart (1986) showed that the February 1974 cyclone developed in a warmer and somewhat more unstable environment than the composite Atlantic storm. According to Rogers and Bosart (1986, their Fig. 4) for the composite Atlantic storm the incipient cyclone central pressure, 1000–500 mb thickness over the cyclone center, 500 mb temperature and geopotential height over the cyclone center, and 700 mb temperature and geopotential height over the cyclone center are: 1000 mb, 543 dam, -23°C, 543 dam, -8°C and 2850 m, respectively. The corresponding numbers for 1200 UTC 16 February 1974 are: 1008 mb, 552 dam, -22°C, 558 dam, -4°C, and 3000 m, respectively. Fig. 6 from Rogers and Bosart (1986) also revealed that kinematic ascent maximized in the 700–500 mb layer to the north and east of the cyclone during the incipient and explosive stage of development. Their finding is consistent with our calculation of deep $\nabla \cdot \boldsymbol{Q} < 0$, maximizing slightly at 850 mb, in the vicinity of the rapidly intensifying cyclone center at 0000 UTC 17 February subject to the important caveat about comparing an individual event with a composite storm.

The February 1974 cyclogenesis event is most analogous to explosive "coiled spring" (Bosart, 1988) development in the extreme western Atlantic ocean during November 1972 as described by Rogers and Bosart (1991). This can be seen by comparing their 500 mb maps for 16–17 November 1972 (their Fig. 2c) with our 500 mb maps (Figs. 3b, e). According to Fig. 7 in Rogers and Bosart (1991) surface θ values near the cyclone center (located slightly farther offshore in November 1972) were ~ 325 K which can be contrasted against an estimated θ of ~ 328 K in the present case based on saturated conditions with a surface temperature of 18°C at a sea level pressure of 1000 mb. Rogers and Bosart (1991) also estimated that surface-based lifted indices were in the 0 to -6 range along and to the right of the track of the November 1972 cyclone which can be contrasted against our estimate of -3 to -4 for air reaching the cyclone center from the southeast. Similarly, their peak observed wind frontogenesis rates (their Fig. 10; same one degree latitude longitude grid as used in this case) of $\sim 30 \times 10^{-10}$°C m^{-1} s^{-1} are very comparable to the peak frontogenesis rates reported for this case. Likewise, the vorticity tendency, dominated by the divergence term, peaked at almost 30×10^{-9} s^{-2} (~ 30 f day^{-1}) which can be contrasted with a peak value of $\sim 15 \times 10^{-9}$ s^{-2} reported by Rogers and Bosart (1991, their Fig. 11).

Our vorticity analysis showed that the ambient relative vorticity in the coastal baroclinic zone was comparable to the value of the local Coriolis parameter during incipient cyclogenesis at 1800 UTC 16 February. The relatively large ambient values of cyclonic relative vorticity in the precyclogenetic environment along the coast occurred in conjunction with coastal frontogenesis as the weakening primary cyclone dissipated to the west of the southern Appalachian Mountains. Consequently, cyclone spinup proceeded rapidly as the horizontal convergence of air at low levels acted on air parcels with a history of cyclonic relative vorticity and these air parcels in turn were ingested into a region of estimated deep tropospheric ascent between the exit region of the southern jet streak and the entrance region of the northern jet streak. The presence of air of near neutral moist static stability in the vicinity of the cyclone center and nearby coastal baroclinic zone probably contributed to the vigor of the ascent associated with the cyclogenesis process and the resulting low level horizontal convergence and cyclonic vorticity generation.

Accordingly, cyclonic vorticity generation near the cyclone center can be viewed as a positive feedback process whereby air parcels with initially large values of ambient absolute vorticity rapidly undergo additional cyclonic vorticity generation when they are stretched vertically in an environment of near neutral moist static stability. This interpretation of cyclonic development, by no means novel, has been used by Palmén and Newton (1969), DiMego and Bosart (1982), Gyakum (1983, 1991), Bosart (1984), Bosart and Lin (1984), Keshishian and Bosart (1987), Holt and Raman (1990), Bosart and Dean (1991), Gyakum et al. (1992), Roebber (1993), and Bullock and Gyakum (1993) among others, to help diagnose and explain cases of explosive continental and marine cyclogenesis. In a related vein Sanders (1986, 1987), Sanders and Davis (1988), Wash et al. (1992), Lupo et al. (1992) and Bullock and Gyakum (1993), among others, have demonstrated that explosively-deepening oceanic cyclones are characterized by stronger troughs and attendant powerful cyclonic vorticity advection in the upper troposphere than are more ordinary cyclones. These results argue for the direct importance of upper tropospheric forcing, as measured by the configuration of the jet streaks for example, on the overall intensity of oceanic cyclogenesis, a conclusion reinforced by this investigation.

A controversial issue in the literature over the last decade has been the role of oceanic sensible and latent heat fluxes, diabatic heating associated with latent heat release from convective and stratiform precipitation, and dry adiabatic heating and cooling in the cyclogenesis process. Danard (1964) was one of the first people to demonstrate the sensitivity of synoptic scale vertical motions to latent heat release and the magnitude of the static stability. Roebber (1984, 1989a) and Gyakum et al. (1989) conducted a statistical climatological investigation of continental versus oceanic cyclones. Their results suggested that the expected normal distribution of cyclone deepening rates was skewed toward greater deepening for explosive oceanic cyclones and that the 24-h period of greatest deepening exhibited modest sensitivity to the gradient of SST as opposed to the magnitude of the SST. Roebber (1989b) used a simple analytical quasi-geostrophic model to illustrate that warm oceanic rings or meanders of order several hundred kilometers in the Gulf Stream had a modest impact on the computed quasi-geostrophic deepening rates. We are suspicious that a similar process may be at work in the present case, given the details of the SST distribution shown in Fig. 1. However, a detailed investigation of the possible impact of the warm oceanic ring in the path of the deepening cyclone in this case is beyond the scope of our present study.

More recently, Lapenta and Seaman (1992) used the Penn State-NCAR mesoscale model to assess the relative importance of adiabatic and diabatic processes to a real data case of cyclogenesis along the east coast of North America. They found that model cyclogenesis was most sensitive to latent heat release associated with widespread precipitation while adiabatic heating and cooling processes and diabatic heating associated with oceanic heat and moisture fluxes played a secondary, but still important, role. A similar conclusion was reached by Kuo et al., 1991, and Reed et al. (1993a, b) in a Penn State-NCAR mesoscale model case study from the Experiment on Rapidly Intensifying Cyclones over the Atlantic (ERICA). On the other hand, Reed and Simmons (1991) and Danard and Ellenton (1980) reported that oceanic cyclogenesis over the western Atlantic Ocean was relatively insensitive to surface sensible and latent heat fluxes in numerical studies of real data cases.

The differences between the various investigations reported in the literature, only a tiny fraction of which have been cited above, may also reflect vagaries in the model resolution and the model physics employed in the sensitivity experiments. For example, Doyle and Warner (1993) showed that the Penn State-NCAR mesoscale model was especially sensitive to the details of the SST temperature distribution and, by inference, the SST gradient. They conducted experiments in which the model was initialized with very high resolution (~ 14 km), intermediate resolution (~ 275 km), and coarse resolution (~ 381 km) SST analyses for a Genesis of Atlantic Lows Experiment (GALE) case study. Their results illustrated a great sensitivity to the details of the mesoscale surface sensible and latent heat fluxes even though the overall heat fluxes differed by only 15% amongst the three experiments. Or to put it another way, the life cycle of model-generated mesoscale disturbances, including the evolution of the model-derived precipitation fields, in the marine boundary layer was highly sensitive to the laplacian of the diabatic heating rates associated with oceanic sensible and latent heating fluxes arising from mesoscale details in the SST field.

In conclusion, our interpretation of the many different studies of oceanic cyclogenesis in the literature is that a broad spectrum of cyclone life cycles is possible. Petterssen et al. (1962), in a study of characteristic Atlantic cyclones, concluded that oceanic surface sensible and latent heat fluxes had little impact on cyclogenesis because these fluxes maximized in the cold air behind the cold front trailing the surface cyclone. The theoretical basis for their argument was that this distribution of oceanic sensible and latent heat fluxes acted to dampen the thermal wave associated with the cyclone, thereby reducing the eddy available potential energy of the large scale flow. This viewpoint was challenged by Bosart (1981) and Bosart and Lin (1984) who demonstrated that oceanic sensible and latent heat fluxes in advance of a coastal cyclone (the infamous Presidents' Day storm of February 1979 along the east coast of North America) played an important role in contributing to the warming, moistening and destabilizing of the air mass flowing westward toward the developing cyclone center to the south of a massive anticyclone. A similar situation was reported by Rogers and Bosart (1991) for the November 1972 cyclone, Jury and Laing (1990) for a South African cyclone, and is also seen to be true in the February 1974 case described above. Additionally, we documented the existence of a narrow band of combined heat and moisture fluxes in excess of 1000 W m^{-2} in a ribbon of storm-force southerly winds immediately ahead of the surface cold front near the apex of the surface cyclone center. We suggest that the role of oceanic sensible and latent heat fluxes on cyclone development is highly case and model dependent and that continuing observational, numerical and theoretical studies will gradually uncover the relevant physical and numerical processes associated with the life cycle of explosive cyclogenesis.

5. Acknowledgement

Anton Seimon is thanked for initially calling our attention to the February 1974 cyclogenesis event. This research was partially supported by NSF grant ATM-8805550 and ONR grant ONR-N00014-88-K-0074.

REFERENCES

Baker, D. G. 1970. *A study of high-pressure ridges to the east of the Appalachian Mountains*. Ph.D. thesis, Massachusetts Institute of Technology, 127 pp. [Available from the Dept. of Meteorology, MIT, Cambridge, MA 02139.]

Beebe, R. G. and Bates, F. C. 1955. A mechanism for assisting in the release of convective instability. *Mon. Wea. Rev.* **83**, 1–10.

Bell, G. D. and Bosart, L. F. 1988. Appalachian cold-air damming. *Mon. Wea. Rev.* **116**, 137–161.

Bell, G. D. and Bosart, L. F. 1989. The large scale atmospheric structure accompanying New England coastal frontogenesis and associated North American cyclogenesis. *Quart. J. Roy. Meteor. Soc.* **115**, 1133–1146.

Bengtsson, L. 1990. Advances in Numerical Prediction of the Atmospheric Circulation in the Extratropics. *Extratropical cyclones*, Palmén Memorial Volume, C. W. Newton and E. O. Holopainen (eds.). Amer. Meteor. Soc., 193–220.

Bluestein, H. 1992. *Synoptic-dynamic meteorology in midlatitudes*, vol. I. *Principles of kinematics and dynamics*. Oxford University Press, 431 pp.

Bosart, L. F. 1975. New England coastal frontogenesis. *Quart. J. Roy. Met. Soc.* **101**, 957–978.

Bosart, L. F. 1981. The Presidents' Day snowstorm of 18–19 February 1979: a subsynoptic-scale event. *Mon. Wea. Rev.* **109**, 1542–1566.

Bosart, L. F. 1984. The Texas coastal rainstorm of 17–21 September 1979: an example of synoptic-mesoscale interaction. *Mon. Wea. Rev.* **112**, 1108–1133.

Bosart, L. F. 1988. Synoptic aspects of cyclogenesis. Seminar proceedings, *The Nature and Prediction of Extratropical Weather Systems*, 7–11 September 1987. European Centre for Medium-Range Weather Forecasts, Volume 1, 17–69.

Bosart, L. F., Vaudo, C. and Helsdon, J. H. Jr. 1972. Coastal frontogenesis. *J. Appl. Meteor.* **11**, 1236–1258.

Bosart, L. F. and Lin, S. C. 1984. A diagnostic analysis of the Presidents' Day storm of February 1979. *Mon. Wea. Rev.* **112**, 2148–2177.

Bosart, L. F. and Dean, D. B. 1991. An analysis of surface features associated with cyclonic redevelopment to the west of tropical storm Agnes in June 1972. *Weather and Forecasting* **6**, 515–537.

Browning, K. A. 1990. Organization of Clouds and Precipitation in Extratropical Cyclones. *Extratropical cyclones*, Palmén Memorial Volume, C. W. Newton and E. O. Holopainen (eds.). Amer. Meteor. Soc., 129–153.

Bullock, T. A. and Gyakum, J. R. 1993. A diagnostic study of cyclogenesis in the western North Pacific ocean. *Mon. Wea. Rev.* **121**, 65–75.

Danard, M. B. 1964. On the influence of released latent heat on cyclone development. *J. Appl. Meteor.* **21**, 261–269.

Danard, M. B. and Ellenton, G. E. 1980. Physical influences on East Coast cyclogenesis. *Atmosphere-Ocean* **18**, 65–82.

DiMego, G. J. and Bosart, L. F. 1982. The transformation of tropical storm Agnes into an extratropical cyclone. Part II: Moisture, Vorticity and kinetic energy budgets. *Mon. Wea. Rev.* **110**, 412–433.

Doyle, J. D. and Warner, T. T. 1993. The impact of the sea surface temperature resolution on mesoscale coastal processes during GALE IOP 2. *Mon. Wea. Rev.* **121**, 313–334.

Forbes, G. S., Anthes, R. A. and Thomas, D. W. 1987. Synoptic and mesoscale aspects of an Appalachian ice storm associated with cold-air damming. *Mon. Wea. Rev.* **115**, 564–591.

Gulf Stream, 1974a. Monthly Summary, United States Naval Oceanographic Office, Washington, DC 20373, vol. 9, no. 1, 6 pp.

Gulf Stream, 1974b. *Ibid*, vol. 9, no. 2, 6 pp.

Gyakum, J. R. 1983. On the evolution of the QE II storm I: Synoptic aspects. *Mon. Wea. Rev.* **111**, 1137–1155.

Gyakum, J. R. 1991. Meteorological precursors to the explosive intensification of the QE II storm. *Mon. Wea. Rev.* **119**, 1105–1131.

Gyakum, J. R., Anderson, J. R., Grumm, R. H. and Gruner, E. L. 1989. North Pacific cold-season surface cyclone activity: 1975–1983. *Mon. Wea. Rev.* **117**, 1141–1155.

Gyakum, J. R., Roebber, P. J. and Bullock, T. A. 1992. The role of antecedent surface vorticity development as a conditioning process in explosive cyclone intensification. *Mon. Wea. Rev.* **120**, 1465–1489.

Holt, T. and Raman, S. 1990. Marine boundary-layer structure and circulation in the region of offshore redevelopment of a cyclone during GALE. *Mon. Wea. Rev.* **118**, 392–410.

Holton, J. R. 1992. *An introduction to dynamic meteorology*, 3rd edition. Academic Press, 511 pp.

Hoskins, B. J. 1990. Theory of extratropical cyclones. *Extratropical cyclones*, Palmén Memorial Volume, C. W. Newton and E. O. Holopainen (eds.). Amer. Meteor. Soc., 63–80.

Hoskins, B. J., Draghici, I. D. and Davies, H. C. 1978. A new look at the omega equation. *Quart. J. Roy. Meteor. Soc.* **104**, 31–38.

Hoskins, B. J. and Pedder, M. A. 1980. The diagnosis of middle latitude synoptic development. *Quart. J. Roy. Meteor. Soc.* **106**, 707–719.

Hoskins, B. J., McIntyre, M. E. and Robertson, A. W. 1985. On the use and significance of isentropic potential vorticity maps. *Quart. J. Roy. Meteor. Soc.* **111**, 877–946.

Jury, M. and Laing, M. 1990. A case study of marine cyclogenesis near Cape Town. *Tellus* **42A**, 246–258.

Keshishian, L. G. and Bosart, L. F. 1987. A case study of extended East Coast frontogenesis. *Mon. Wea. Rev.* **115**, 100–117.

Kocin, P. J. and Uccellini, L. W. 1990. Snowstorms along the northeastern coast of the United States, 1955–1985. *Meteor. Monogr.* **22**, no. 44, 280 pp.

Kuo, Y.-H., Reed, R. J. and Low-Nam, S. 1991. Effects of surface energy fluxes during the early development and rapid intensification stages of seven explosive cyclones in the western Atlantic. *Mon. Wea. Rev.* **119**, 457–476.

Lapenta, W. M. and Seaman, N. L. 1992. A numerical investigation of East Coast cyclogenesis during the cold-air damming event of 27–28 February 1982. Part II: Importance of physical mechanisms. *Mon. Wea. Rev.* **120**, 52–76.

Lupo, A. R., Smith, P. J. and Zwack, P. 1992. A diagnosis of the explosive development of two extratropical cyclones. *Mon. Wea. Rev.* **120**, 1490–1523.

Miller, J. E. 1948. On the concept of frontogenesis. *J. of Meteor.* **5**, 169–171.

Neiman, P. J. and Shapiro, M. A. 1993. The life cycle of an extratropical marine cyclone. Part I: Frontal cyclone evolution and thermodynamic air sea interaction. *Mon. Wea. Rev.* **121**, 2153–2176.

Neiman, P. J., Shapiro, M. A. and Fedor, L. S. 1993. The life cycle of an extratropical marine cyclone. Part II: Mesoscale structure and diagnostics. *Mon. Wea. Rev.* **121**, 2177–2199.

O'Handley, C. and Bosart, L. F. 1989. Subsynoptic-scale structure in a major synoptic-scale cyclone. *Mon. Wea. Rev.* **117**, 607–630.

Palmén, E. and Newton, C. W. 1969. *Atmospheric circulation systems: their structure and physical interpretation.* Academic Press, 603 pp.

Petterssen, S., Bradbury, D. L. and Pedersen, K. 1962. The Norwegian cyclone models in relation to heat and cold sources. *Geofys. Publ.* **24**, 243–280.

Reed, R. J. 1990. Advances in knowledge and understanding of extratropical cyclones during the past quarter centery: an overview. *Extratropical cyclones*, Palmén Memorial Volume, C. W. Newton and E. O. Holopainen (eds.). Amer. Meteor. Soc., 27–45.

Reed, R. J. and Simmons, A. J. 1991. Numerical simulation of an explosively deepening cyclone over the North Atlantic that was unaffected by concurrent surface energy fluxes. *Wea. Forecasting* **6**, 117–122.

Reed, R. J., Grell, G. A. and Kuo, Y.-H. 1993a. The ERICA IOP5 Storm. Part I: Analysis and simulation. *Mon. Wea. Rev.* **121**, 1577–1594.

Reed, R. J., Grell, G. A. and Kuo, Y.-H. 1993b. The ERICA IOP5 Storm. Part II: Sensitvity tests and further diagnosis based on model output. *Mon. Wea. Rev.* **121**, 1595–1612.

Richwein, B. A. 1980. The damming effect of the southern Appalachians. *Natl. Wea. Dig.* **5**, 2–12.

Riordan, A. J. 1990. Examination of the mesoscale features of the GALE Coastal Front of 24–25 January 1986. *Mon. Wea. Rev.* **118**, 258–282.

Roebber, P. J. 1984. Statistical analysis and updated climatology of explosive cyclones. *Mon. Wea. Rev.* **112**, 1577–1589.

Roebber, P. J. 1989a. On the statistical analysis of cyclone deepening rates. *Mon. Wea. Rev.* **117**, 2293–2298.

Roebber, P. J. 1989b. The role of heat and moisture fluxes associated with large-scale ocean current meanders in maritime cyclogenesis. *Mon. Wea. Rev.* **117**, 1676–1694.

Roebber, P. J. 1993. A diagnostic case study of self-development as an antecedent conditioning process in explosive cyclogenesis. *Mon. Wea. Rev.* **121**, 976–1006.

Rogers, E. and Bosart, L. F. 1986. An investigation of explosively deepening oceanic cyclones. *Mon. Wea. Rev.* **114**, 702–718.

Rogers, E. and Bosart, L. F. 1991. A diagnostic study of two intense oceanic cyclones. *Mon. Wea. Rev.* **119**, 967–997.

Sanders, F. 1986. Explosive cyclogenesis over the West-Central North Atlantic Ocean, 1981–84. Part I: Composite structure and mean behavior. *Mon. Wea. Rev.* **114**, 1781–1794.

Sanders, F. 1987. A study of 500 mb vorticity maxima crossing the East Coast of North American and associated surface cyclogenesis. *Wea. Forecasting* **2**, 70–83.

Sanders, F. and Gyakum, J. R. 1980. Synoptic-dynamic climatology of the "bomb". *Mon. Wea. Rev.* **108**, 1589–1606.

Sanders, F. and Davis, C. A. 1988. Patterns of thickness anomaly for explosive cyclogenesis over the west-central North Atlantic Ocean. *Mon. Wea. Rev.* **116**, 2725–2730.

Shapiro, M. A. and Keyser, D. 1990. Fronts, jet streams and the tropopause. *Extratropical cyclones*, Palmén Memorial Volume, C. W. Newton and E. O. Holopainen (eds.). Amer. Meteor. Soc. 167–191.

Stauffer, D. R. and Warner, T. T. 1987. A numerical study of Appalachian cold-air damming and coastal frontogenesis. *Mon. Wea. Rev.* **115**, 799–821.

Sutcliffe, R. C. and Forsdyke, A. G. 1950. The theory and use of upper air thickness patterns in forecasting. *Quart. J. Roy. Meteor. Soc.* **76**, 189–217.

Tracton, M. S. 1973. The role of cumulus convection in the development of extratropical cyclones. *Mon. Wea. Rev.* **101**, 573–593.

Uccellini, L. W. 1990. Processes contributing to the rapid development of extratropical cyclones. *Extratropical cyclones*, Palmén Memorial Volume, C. W. Newton and E. O. Holopainen (eds.), Amer. Meteor. Soc., 81–105.

Uccellini, L. W. and Johnson, D. R. 1979. The coupling of upper and lower tropospheric jet streaks and implications for the development of severe convective storms. *Mon. Wea. Rev.* **107**, 682–703.

Uccellini, L. W., Keyser, D., Brill, K. F. and Wash, D. H. 1985. The Presidents' Day cyclone of February 1979: Influence of upstream trough amplification and associated tropopause folding on rapid cyclogenesis. *Mon. Wea. Rev.* **113**, 962–988.

Uccellini, L. W. and Kocin, P. J. 1987. The interaction of jet streak circulations during heavy snow events along the East Coast of the United States. *Wea. Forecasting* **2**, 289–308.

Uccellini, L. W., Petersen, R. A., Brill, K. F., Kocin, P. J. and Tuccillo, J. J. 1987. Synergistic interactions between an upper-level jet streak and diabatic processes that influence the development of a low-level jet and a secondary coastal cyclone. *Mon. Wea. Rev.* **115**, 2227–2261.

Wash, C. H., Hale, R. A., Dobos, P. H. and Wright, E. J. 1992. Study of explosive and nonexplosive cyclogenesis during FGGE. *Mon. Wea. Rev.* **120**, 40–51.